REPORT NO.
UCB/SESM-76/04

STRUCTURAL ENGINEERING
AND STRUCTURAL MECHANICS

FINITE ELEMENT FORMULATION AND SOLUTION OF CONTACT - IMPACT PROBLEMS IN CONTINUUM MECHANICS - IV

BY

Thomas J. Hughes
Robert L. Taylor
Jerome L. Sackman
and
Worsak Kanoknukulchai

JULY 1976

DEPARTMENT OF CIVIL ENGINEERING
UNIVERSITY OF CALIFORNIA
BERKELEY, CALIFORNIA

Table of Contents

Acknowledgment

This report was prepared under Subcontract No. N68305-75-C-004; sponsored by Civil Engineering Laboratory, Naval Construction Battalion Center, Port Hueneme, California as part of NHSTA Interagency Agreement Number DOT-HS-5-01235, funded by the National Highway Traffic Safety Administration of the Department of Transportation, and Funding Document Number ONR 76-WR-60083, funded by the Office of Naval Research.

The opinions, findings and conclusions expressed in this publication are those of the authors and not necessarily those of the Civil Engineering Laboratory, the National Highway Traffic Safety Administration, or the Office of Naval Research.

Introduction

In this report we describe work completed under Subcontract No. N68305-75-C-004 (Proposal UCB-Eng.-3889). As we frequently refer to our previous work [1-5], it will prove helpful to the reader to be somwhat familiar with these references.

In Section I we present theory and algorithms for large displacement contact-impact analysis in two dimensions(i.e. plane stress, plane strain and axisymmetric). This work builds upon earlier developments documented in [2] and [3] and represents the completion of our theoretical work in this area. The theory encompasses a wide range of contact-impact problems and allows for a completely arbitrary contact surface development, stick, slip and frictional sliding conditions, and impact-release conditions covering the full range of contact possibilities.

In Section II we describe some new developments regarding the Hertzian algorithm, which has been extensively documented in previous publications; see [1-5].

Section III contains sample problems which employ the algorithms described in Section I and also some studies involving the Hertzian algorithm.

Anticipating the need for an efficient shell element for crash configuration modelling, we have performed a pilot study of a plate bending element. The results of this study, which are encouraging, are contained in Section IV.

I. Large Displacement Contact-Impact Theory

1. Introduction

In the following sections we present a large displacement contact-impact theory. In Section I-2 we set notations and establish the structure of the local equations for a typical contactor node and target element boundary. The algorithm for handling stick, slip and frictional contact conditions is discussed in Section I-3. This strategy is sufficient for the quasi-static problem and governs the iterations within a time step in a dynamic problem. The updating in dynamic problems manifested by discrete impact-release conditions is described in Section I-4.

2. Local Structure of the Equations

To explicate the structure of the equations we wish to solve, we shall consider in this section an idealization consisting of one contactor node and one target element boundary (see Fig. I-1). Quantities associated with the contactor node will possess a subscript k, and those associated with the target nodes will possess a subscript ℓ or $\ell+1$. Throughout this section we shall concern ourselves only with equations which pertain to these three nodes. In two-dimensional analysis (i.e. plane stress, plane strain or axisymmetric) there are two displacement degrees-of-freedom associated with each of the three nodes and, in addition, two contact force degrees-of-freedom associated to the contactor node; a total of eight degrees-of-freedom for the three nodes considered here. Thus there are six equations of motion to be satisfied and, if the bodies are in contact, two conditions of compatibility. Consider the case in which the contactor node is in contact with the target element boundary. Then if α is the nondimensional location parameter for the target element boundary, defined by (see Fig. I-2):

$$\alpha = [(x_{1k} - x_{1\ell})^2 + (x_{2k} - x_{2\ell})^2]^{1/2} / L ,$$

$$L = [(x_{1,\ \ell+1} - x_{1\ell})^2 + (x_{2,\ \ell+1} - x_{2\ell})^2]^{1/2} ,$$

the eight equations to be satisfied for the three nodes are:

$$\begin{bmatrix} \underset{\sim}{m} & \underset{\sim}{o} \\ \underset{\sim}{o} & \underset{\sim}{m} \end{bmatrix} \begin{bmatrix} \ddot{\underset{\sim}{y}}_1 \\ \ddot{\underset{\sim}{y}}_2 \end{bmatrix} + \begin{bmatrix} \underset{\sim}{k}_1 \\ \underset{\sim}{k}_2 \end{bmatrix} + \begin{bmatrix} \hat{\underset{\sim}{\tau}}_1 \\ \hat{\underset{\sim}{\tau}}_2 \end{bmatrix} + \begin{bmatrix} \hat{\underset{\sim}{x}}_1 \\ \hat{\underset{\sim}{x}}_2 \end{bmatrix} = \underset{\sim}{o} \qquad \text{(I-1)}$$

where

$$\underset{\sim}{m} = \begin{bmatrix} M^1_k & o & o & o \\ o & o & o & o \\ o & o & M^2_\ell & o \\ o & o & o & M^2_{\ell+1} \end{bmatrix}, \text{ the } \underline{\text{mass}},$$

$$\underset{\sim}{y}_\gamma = (u^1_{\gamma k} \quad o \quad u^2_{\gamma \ell} \quad u^2_{\gamma,\ell+1})^T, \text{ the } \underline{\text{displacements}},$$

$$\underset{\sim}{k}_\gamma = (K^1_{\gamma k} \quad o \quad K^2_{\gamma \ell} \quad K^2_{\gamma,\ell+1})^T, \text{ the } \underline{\text{internal forces}},$$

$$\underset{\sim}{\tau}_\gamma = (\tau_{\gamma k} \quad o \quad -(1-\alpha)\tau_{\gamma k} \quad -\alpha\, \tau_{\gamma k})^T, \text{ the } \underline{\text{contact forces}},$$

and

$$\underset{\sim}{\hat{x}}_\gamma = (o \ \{x^1_{\gamma k} - (1-\alpha)\, x^2_{\gamma \ell} - \alpha x^2_{\gamma,\, \ell+1}\} \quad o \quad o \quad)^T,$$

the <u>compatibility conditions</u>. The superscript indicates to which body the quantity pertains and the subscript γ indicates the coordinate direction z_γ, $\gamma = 1,2$. Note that the components K^1 and K^2 are functions of the displacements of B^1 and B^2, respectively.

The compatibility conditions amount to the second and sixth equations in I-1. When the bodies are not in contact these conditions are ignored and $\tau_{\gamma k} = o$.

The solution of the matrix equations is developed by employing a temporal discretization which results in a nonlinear algebraic problem to be solved at each time step. The Newmark family of algorithms is employed by us to temporally discretize the equations and we confine our attention to implicit methods. This aspect of our work has been described previously (see e.g. [5]) and we shall not repeat the details here. The resulting temporally discretized system, for the nodes in question, becomes:

$$\frac{1}{\beta\,\Delta t^2}\begin{bmatrix} \underset{\sim}{m} & \underset{\sim}{o} \\ \underset{\sim}{o} & \underset{\sim}{m} \end{bmatrix}\begin{bmatrix} \underset{\sim}{y}_1 \\ \underset{\sim}{y}_2 \end{bmatrix}_{n+1} + \begin{bmatrix} \underset{\sim}{k}_1 \\ \underset{\sim}{k}_2 \end{bmatrix}_{n+1} + \begin{bmatrix} \hat{\underset{\sim}{\tau}}_1 \\ \hat{\underset{\sim}{\tau}}_2 \end{bmatrix}_{n+1}$$

$$+ \begin{bmatrix} \hat{\underset{\sim}{x}}_1 \\ \hat{\underset{\sim}{x}}_2 \end{bmatrix}_{n+1} = \begin{bmatrix} \underset{\sim}{m} & \underset{\sim}{o} \\ \underset{\sim}{o} & \underset{\sim}{m} \end{bmatrix}\left(\frac{1}{\beta\,\Delta t^2}\begin{bmatrix} \underset{\sim}{y}_1 \\ \underset{\sim}{y}_2 \end{bmatrix}_n + \frac{1}{\beta\,\Delta t}\begin{bmatrix} \dot{\underset{\sim}{y}}_1 \\ \dot{\underset{\sim}{y}}_2 \end{bmatrix}_n \right. \tag{I-2}$$

$$\left. + \frac{1-2\beta}{2\beta}\begin{bmatrix} \ddot{\underset{\sim}{y}}_1 \\ \ddot{\underset{\sim}{y}}_2 \end{bmatrix}_n \right) ,$$

where the subscripts n and n+1 indicate the time step at which the quantity is evaluated, $\Delta t = t_{n+1} - t_n$ is the length of the time interval, and β is the Newmark parameter.

To solve the nonlinear algebraic problem at each time step, the Newton-Raphson method is employed. The linear equations used in this procedure, for the nodes in question, are given as follows:

$$\underset{\sim}{k}^* \, \Delta \underset{\sim}{w}_{n+1}^{(i)} = \underset{\sim}{r}^* , \tag{I-3}$$

where

$$\underset{\sim}{k}^* = \frac{1}{\beta\,\Delta t^2}\begin{bmatrix} \underset{\sim}{m} & \underset{\sim}{o} \\ \underset{\sim}{o} & \underset{\sim}{m} \end{bmatrix} + D\begin{bmatrix} \underset{\sim}{k}_1 \\ \underset{\sim}{k}_2 \end{bmatrix}_{n+1} + \begin{bmatrix} \underset{\sim}{\alpha}_1 & \underset{\sim}{o} \\ \underset{\sim}{o} & \underset{\sim}{\alpha}_2 \end{bmatrix}^{(i)} ,$$

$$\underset{\sim}{r}^{*} = -\begin{bmatrix} \underset{\sim}{k}_1 \\ \underset{\sim}{k}_2 \end{bmatrix}^{(i)}_{n+1} - \begin{bmatrix} \hat{\underset{\sim}{\tau}}_1 \\ \hat{\underset{\sim}{\tau}}_2 \end{bmatrix}^{(i)}_{n+1} - \begin{bmatrix} \hat{\underset{\sim}{x}}_1 \\ \hat{\underset{\sim}{x}}_2 \end{bmatrix}^{(i)}_{n+1}$$

$$+ \begin{bmatrix} \underset{\sim}{m} & \underset{\sim}{o} \\ \underset{\sim}{o} & \underset{\sim}{m} \end{bmatrix} \left(\frac{1}{\beta\ \Delta t^2} \begin{bmatrix} \underset{\sim}{y}_1 \\ \underset{\sim}{y}_2 \end{bmatrix}_n + \frac{1}{\beta\ \Delta t} \begin{bmatrix} \dot{\underset{\sim}{y}}_1 \\ \dot{\underset{\sim}{y}}_2 \end{bmatrix}_n \right.$$

$$\left. + \frac{1-2\beta}{2\beta} \begin{bmatrix} \ddot{\underset{\sim}{y}}_1 \\ \ddot{\underset{\sim}{y}}_2 \end{bmatrix}_n - \frac{1}{\beta\ \Delta t^2} \begin{bmatrix} \underset{\sim}{y}_1 \\ \underset{\sim}{y}_2 \end{bmatrix}^{(i)}_{n+1} \right) .$$

where the superscript in parentheses indicates the iteration number and

$$D \begin{bmatrix} \underset{\sim}{k}_1 \\ \underset{\sim}{k}_2 \end{bmatrix}$$

denotes the tangent stiffness matrix. The formation of the tangent stiffness follows the standard rules (in particular, in the case of linear elastic bodies it is the usual stiffness matrix). The iterative process is defined by

$$\underset{\sim}{w}^{(o)}_{n+1} = \underset{\sim}{w}_n ,$$

$$\underset{\sim}{w}^{(i+1)}_{n+1} = \underset{\sim}{w}^{(i)}_{n+1} + \Delta \underset{\sim}{w}^{(i)}_{n+1} ,$$

and when $\underset{\sim}{w}^{(i)}_{n+1}$ satisfies a convergence test, for some i, then $\underset{\sim}{w}_{n+1} \overset{\text{def.}}{=} \underset{\sim}{w}^{(i)}_{n+1}$. Here $\underset{\sim}{w}$ is defined by

$$\underset{\sim}{w} = \begin{bmatrix} \underset{\sim}{y}_1 \\ \underset{\sim}{y}_2 \end{bmatrix} + (o \quad \tau_{1k} \quad o \quad o \quad o \quad \tau_{2k} \quad o \quad o \quad)^T .$$

The matrix

$$\begin{bmatrix} \underset{\sim}{\alpha}_1 & \underset{\sim}{0} \\ \underset{\sim}{0} & \underset{\sim}{\alpha}_2 \end{bmatrix}$$

is called the contact stiffness. Specification of it,

$$\begin{bmatrix} \hat{\underset{\sim}{\tau}}_1 \\ \hat{\underset{\sim}{\tau}}_2 \end{bmatrix}^{(i)}_{n+1} \quad \text{and} \quad \begin{bmatrix} \hat{\underset{\sim}{x}}_1 \\ \hat{\underset{\sim}{x}}_2 \end{bmatrix}^{(i)}_{n+1}$$

are the unique aspects of the contact-impact algorithm. In the next section we describe the way this is done.

In passing, we note that formally setting $\underset{\sim}{m}$ to $\underset{\sim}{0}$ provides an algorithm for the quasi-static case.

3. Computing Strategy Within a Time (Load) Step

In this section we describe the strategy involved in solving the non-linear algebraic contact problem within a time step (or, equivalently, within a load step in the quasi-static case). The unknowns involved, as described in the previous section, are the displacements and contact forces at the end of the step. Treatment of velocities and accelerations, and updating of contact forces, when impact and release effects are present, are considered in the following section.

For consideration of sliding contact, it is convenient to work in a coordinate system naturally defined by the target segment. A system of this kind can be constructed by aligning the coordinate axes in the tangential (s) and normal (n) directions to the target element boundary, with origin located at node ℓ (see Fig. I-3). If θ denotes the angle between the s and z_1 axes, measured counterclockwise from z_1, then

$$\theta = \arctan\left[(x_{2,\,\ell+1} - x_{2\ell})/(x_{1,\,\ell+1} - x_{1\ell})\right] ,$$

and vectors may be resolved in the usual way into tangential and normal components, e.g.

$$\begin{bmatrix} \tau_s \\ \tau_n \end{bmatrix} = \begin{bmatrix} c & s \\ -s & c \end{bmatrix} \begin{bmatrix} \tau_1 \\ \tau_2 \end{bmatrix}$$

where $c = \cos\theta$ and $s = \sin\theta$. Thus the vectors in the s, n - system corresponding to $\hat{\underset{\sim}{\tau}}_1$ and $\hat{\underset{\sim}{\tau}}_2$ are

$$\hat{\underset{\sim}{\tau}}_s = (\tau_{sk} \quad o \quad -(1-\alpha)\tau_{sk} \quad -\alpha\,\tau_{sk})^T \qquad \text{and}$$

$$\hat{\underset{\sim}{\tau}}_n = (\tau_{nk} \quad o \quad -(1-\alpha)\tau_{nk} \quad -\alpha\,\tau_{nk})^T ,$$

respectively, and likewise for $\hat{\underset{\sim}{x}}_s$ and $\hat{\underset{\sim}{x}}_n$.

At the end of each iteration, one of three conditions can hold for a typical contactor node k; the condition is determined by the contactor code i_k. If $i_k = o$, then contactor node k is not in contact; if $i_k > o$, then node k is in contact. The code $i_k = 1$ signifies the stick condition and $i_k = 2$ signifies the sliding condition. The contact code determines what is assembled into the contact stiffness and the right-hand side vectors $\underset{\sim}{\tau}$ and $\hat{\underset{\sim}{x}}$. Specifically, we have the following situations:

$i_k = o$:

$$\underset{\sim}{\alpha}_\gamma = \underset{\sim}{\beta}$$

$$\hat{\underset{\sim}{\tau}}_\gamma^{(i)} = \underset{\sim}{o}$$

$$\hat{\underset{\sim}{x}}_\gamma^{(i)} = \underset{\sim}{o}$$

$i_k = 1$:

$$\underset{\sim}{\alpha}_\gamma = \underset{\sim}{\alpha}$$

$$\hat{\underset{\sim}{\tau}}_\gamma^{(i)} \leftarrow \hat{\underset{\sim}{\tau}}_\gamma^{(i)} + \Delta\hat{\underset{\sim}{\tau}}_\gamma^{(i)}$$

$$\hat{\underset{\sim}{x}}_\gamma^{(i)} \leftarrow \hat{\underset{\sim}{x}}_\gamma^{(i)} + \Delta\hat{\underset{\sim}{x}}_\gamma^{(i)}$$

$i_k = 2$:

$$\underset{\sim}{\alpha}_s = \underset{\sim}{\beta}$$

$$\underset{\sim}{\alpha}_n = \underset{\sim}{\alpha}$$

$$\hat{\underset{\sim}{\tau}}_n^{(i)} \leftarrow \hat{\underset{\sim}{\tau}}_n^{(i)} + \Delta\hat{\underset{\sim}{\tau}}_n^{(i)}$$

$$\hat{\underset{\sim}{\tau}}_s^{(i)} \leftarrow f_d \operatorname{sgn}\left(\tau_{sk}^{(i)} + \Delta\tau_{sk}^{(i)}\right)\left|\hat{\underset{\sim}{\tau}}_n^{(i)}\right|$$

$$\hat{\underset{\sim}{x}}_s^{(i)} \leftarrow \underset{\sim}{o}$$

$$\hat{\underset{\sim}{x}}_n^{(i)} \leftarrow \hat{\underset{\sim}{x}}_n^{(i)} + \Delta\hat{\underset{\sim}{x}}_n^{(i)}$$

where

$$\underset{\sim}{\alpha} = \begin{bmatrix} 0 & 1 & 0 & 0 \\ 1 & 0 & -(1-\alpha) & -\alpha \\ 0 & -(1-\alpha) & 0 & 0 \\ 0 & -\alpha & 0 & 0 \end{bmatrix}$$

$$\beta = \begin{bmatrix} 0 & 0 & 0 & 0 \\ 0 & 1 & 0 & 0 \\ 0 & 0 & 0 & 0 \\ 0 & 0 & 0 & 0 \end{bmatrix}$$

$$|\hat{\underset{\sim}{\tau}}_n| = (|\tau_{nk}| \quad 0 \quad -(1-\alpha) \mid \tau_{nk} \mid -\alpha \mid \tau_{nk} \mid)^T$$

and f_d is the dynamic coefficient of friction. Rotation of quantities in local coordinates into global coordinates is facilitated by the following transformations:

$$\begin{bmatrix} \underset{\sim}{\alpha}_1 & \underset{\sim}{0} \\ \underset{\sim}{0} & \underset{\sim}{\alpha}_2 \end{bmatrix} = \underset{\sim}{T}^T \begin{bmatrix} \underset{\sim}{\alpha}_s & \underset{\sim}{0} \\ \underset{\sim}{0} & \underset{\sim}{\alpha}_n \end{bmatrix} \underset{\sim}{T}$$

in which

$$\underset{\sim}{T} = \begin{bmatrix} c & 0 & 0 & 0 & s & 0 & 0 & 0 \\ 0 & c & 0 & 0 & 0 & s & 0 & 0 \\ 0 & 0 & c & 0 & 0 & 0 & s & 0 \\ 0 & 0 & 0 & c & 0 & 0 & 0 & 0 \\ -s & 0 & 0 & 0 & c & 0 & 0 & 0 \\ 0 & -s & 0 & 0 & 0 & c & 0 & 0 \\ 0 & 0 & -s & 0 & 0 & 0 & c & 0 \\ 0 & 0 & 0 & -s & 0 & 0 & 0 & c \end{bmatrix}$$

and

$$\hat{\underset{\sim}{x}}_1 = c\,\hat{\underset{\sim}{x}}_s - s\,\hat{\underset{\sim}{x}}_n$$

$$\hat{\underset{\sim}{x}}_2 = s\,\hat{\underset{\sim}{x}}_s + c\,\hat{\underset{\sim}{x}}_n$$

$$\hat{\underset{\sim}{\tau}}_1 = c\,\hat{\underset{\sim}{\tau}}_s - s\,\hat{\underset{\sim}{\tau}}_n$$

$$\hat{\underset{\sim}{\tau}}_2 = s\,\hat{\underset{\sim}{\tau}}_s + c\,\hat{\underset{\sim}{\tau}}_n \quad .$$

The determination of the contactor code i_k for the present iteration depends upon its value for the previous iteration.

If i_k was equal to o, then node k was not in contact during the previous interation. In this case we must determine whether or not node k has penetrated a target segment during the present iteration. Let $\underset{\sim}{x}_k$ denote the location of node k and let $\underset{\sim}{x}_{\ell-1}$, $\underset{\sim}{x}_\ell$, $x_{\ell+1}$ denote the locations of consecutive target nodes ℓ-1, ℓ, ℓ+1, respectively, where ℓ designates an interior node of some segment. We assume that the entire list of interior target nodes has been searched and k is found to be closest to ℓ at the end of the present iteration. For node ℓ the interior of the target is defined to be that part of the plane consisting of the two straight lines emanating from $\underset{\sim}{x}_\ell$ through $\underset{\sim}{x}_{\ell-1}$ and $\underset{\sim}{x}_{\ell+1}$ and extending to infinity, and all points to the right of these lines with respect to the target direction. The exterior is the remaining portion of the plane (see Fig. I-4). At the end of an iteration, if $\underset{\sim}{x}_k$ is in the interior of the target we say that tentative contact has been made. To determine if this has occurred we employ the following algorithm (see Fig. I-4 for notation).

Let $\underset{\sim}{A} = (\underset{\sim}{x}_k, \underset{\sim}{x}_{\ell-1}, \underset{\sim}{x}_\ell, \underset{\sim}{x}_{\ell+1})$ and define TEST as indicated in Fig. I-5. If the outcome of TEST is true (T), then $\underset{\sim}{x}_k$ is exterior to the target, whereas if the outcome is false (F), $\underset{\sim}{x}_k$ is in the interior and tentative contact has been made. In the latter case further calculations are required

to determine if indeed contact has occurred* and, if so, where. The routine to carry out these calculations requires the input parameters i_{max} and j_{max}, which are the maximum number of iterations allowed to determine the approximate location of a contact point, and the maximum number of changes of target reference node allowed, respectively. If tentative contact has been made we next employ a binary search procedure to determine a good approximation to the configuration $\underline{A}$ at which initial contact was actually made. With this configuration determined, we ascertain whether node k actually contacted the segment defined by target nodes ℓ-1, ℓ, ℓ+1 ($|\alpha| \leq 1$) or did not ($|\alpha| > 1$). In the former case we set the new value of the contactor code i_k to 1, whereas in the latter we may try another reference point and repeat the calculation. However, if j_{max} has been reached, or the new reference point is a target segment boundary node, we assume no contact has been made and set i_k to o.

The following is a brief description of the main points of the flowchart depicted in Figs. I-6 to I-11.

If i_k was greater than zero for the previous iteration, then contactor node k was in contact. In this case it is first checked if the updated normal component of traction τ_n is compressive. If this is not the case, then i_k is set to zero. If τ_n is compressive, then it is determined whether contactor node k was sticking ($i_k = 1$) or whether it was sliding ($i_k = 2$) during the last iteration. If it was sticking then the updated value of $|\tau_s|$ is compared with $\tau_{crit} = f_s |\tau_n|$, where f_s is the static coefficient of friction. If $|\tau_s| \geq \tau_{crit}$, then i_k is set equal to 2; otherwise i_k is set to 1. If node k was sliding during the last iteration then a new value of α is computed based upon the updated configuration. If

*A contactor node can enter the interior without passing through the target, e.g. by sneaking around a boundary node.

$|\alpha| \leq 1$, then $|\tau_s|$ is compared with $\tau_{crit} = f_d\ |\tau_n|$. The result of this comparison determines whether contactor node k is sliding or sticking, as above. If $|\alpha| > 1$, the target reference node is changed to the appropriate adjacent one. A maximum of i_{smax} changes of reference are allowed. (The default value of i_{smax} is one). If i_{smax} is exceeded, the computation is terminated and an error message is printed. If in changing the target reference node a target segment boundary node is encountered, the no contact code i_k is set to zero. If a value of α is found such that $|\alpha| \leq 1$, then $|\tau_s|$ is compared with $\tau_{crit} = f_d\ |\tau_n|$ and we proceed as described above. When contactor nodes slide over target nodes, the computation of the new values of α is approximate, unless the target segment is flat. Thus some caution is advised in application to problems in which substantial sliding is likely during a time (load) step.

4. Impact-Release Conditions

Imposing correct impact and release conditions are essential ingredients in the accurate solution of dynamic contact problems. The present developments extend earlier work (see [1-5]) in which simple node on node normal incidence was considered. In this section we describe procedures for setting impact-release conditions for the stick, slip and frictional cases. Since each of the cases differs somewhat from the others we discuss them one at a time. The stick case is the most straightforward and we shall describe it first.

a. Stick Contact Condition

We consider the case of an open target segment consisting of N^2 nodes (the superscript refers to body number 2). The case of a closed target follows trivially. We allow for the possibility of an arbitrary number of contactor nodes impacting and/or releasing the target segment over the time step. The updating of nodal velocities is determined from the following two conditions:

(1) The velocity of a contactor node in contact with the target segment is the linear interpolate of the target node velocities of the element boundary in question. For instance, consider the configuration of Fig. I-2 in which contactor node k is in contact with the element boundary defined by target nodes ℓ and $\ell+1$. In this section we will attach a subscript to the nondimensional location parameter to indicate that it is associated with contactor node k, i.e. we denote it α_k. If $\dot{\underset{\sim}{u}}_k$ denotes the velocity vector of contactor node k, and $\dot{\underset{\sim}{u}}_\ell$ and $\dot{\underset{\sim}{u}}_{\ell+1}$ are the velocity vectors of target nodes ℓ and $\ell+1$, respectively, then the condition of linear interpolation requires

$$\dot{\underset{\sim}{u}}_k = (1-\alpha_k)\dot{\underset{\sim}{u}}_\ell + \alpha_k \dot{\underset{\sim}{u}}_{\ell+1} \qquad \text{(I-4)}$$

Observe that this definition remains meaningful when there are more than one contactor nodes in contact with a single element boundary.

(2) The second condition is a discrete impulse-momentum balance. Let A_ℓ denote the tributary area surrounding target node ℓ. Specifically, this area is defined to be one-half the length of the two adjacent target element boundaries to node ℓ, in case node ℓ is an interior node; and one-half the length of the adjacent target segment, if node ℓ is a target segment boundary node (see Fig. I-12). Let C_ℓ^- denote the set of contactor nodes in contact with A_ℓ at the end of the time step (last iteration), and let C_ℓ^{-1} denote the set of contactor nodes which were in contact with A_ℓ at the beginning of the time step, but which released during the time step. Then for each $\ell \in \{1,2,\ldots,N^2\}$ we require that

$$M_\ell^t \, \dot{\underset{\sim}{u}}_\ell^{-1} + \sum_{k \in C_\ell^-} M_k^c \, \dot{\underset{\sim}{u}}_k^{-1} + \frac{\Delta t}{2} \sum_{k \in C_\ell^{-1}} \underset{\sim}{\tau}_k^{-1}$$

$$= M_\ell^t \, \dot{\underset{\sim}{u}}_\ell^{+} + \sum_{k \in C_\ell^-} M_k^c \, \dot{\underset{\sim}{u}}_k^{+} \quad , \tag{I-5}$$

and for each $k \in C_\ell^{-1}$ we require

$$M_k^c \, \dot{\underset{\sim}{u}}_k^{+} = M_k^c \, \dot{\underset{\sim}{u}}_k^{-1} - \frac{\Delta t}{2} \, \underset{\sim}{\tau}_k^{-1} \quad , \tag{I-6}$$

where the superscripts + and -1 indicate the updated values and values from the previous time step, respectively, M_ℓ^t indicates the lumped mass coefficient of target node ℓ and M_k^c is the lumped mass coefficient of contactor node k.

Equation (I-6) defines $\dot{\underset{\sim}{u}}_k^{+}$ for all $k \in C_\ell^{-1}$, in terms of the data from the previous step; namely $\dot{\underset{\sim}{u}}_k^{-1}$ and $\underset{\sim}{\tau}_k^{-1}$. Equations (6.1) and (6.2) lead to the following system of equations for the target nodal velocities:

$$\underset{\sim}{A} \, \dot{\underset{\sim}{U}} = \underset{\sim}{B} \tag{I-7}$$

where A is tridiagonal with nonzero coefficients

$$a_{\ell,\,\ell-1} = \sum_{k\in(C_\ell^-)_{left}} M_k^c(1-\alpha_k),\quad \ell\in\{2,3,\ldots,N^2\}$$

$$a_{\ell,\ell} = M^t + \sum_{k\in(C_\ell^-)_{left}} M_k^c\,\alpha_k + \sum_{k\in(C_\ell^-)_{right}} M_k^c(1-\alpha_k),\quad \ell\in\{1,2,3,\ldots N^2\}$$

$$a_{\ell,\,\ell+1} = \sum_{k\in(C_\ell^-)_{right}} M_k^c\,\alpha_k,\quad \ell\in\{1,2,3,\ldots N^2-1\}$$

and

$$\underset{\sim}{\dot{U}} = \begin{bmatrix} \dot{u}_{11}^+ & \dot{u}_{12}^+ \\ \dot{u}_{21}^+ & \dot{u}_{22}^+ \\ \cdot & \cdot \\ \cdot & \cdot \\ \cdot & \cdot \\ \dot{u}_{N^2 1}^+ & \dot{u}_{N^2 2}^+ \end{bmatrix} \qquad \underset{\sim}{B} = \begin{bmatrix} b_{11} & b_{12} \\ b_{21} & b_{22} \\ \cdot & \cdot \\ \cdot & \cdot \\ \cdot & \cdot \\ b_{N^2 1} & b_{N^2 2} \end{bmatrix}$$

in which

$$\underset{\sim}{b}_\ell = M_\ell^t\,\underset{\sim}{\dot{u}}_\ell^{-1} + \sum_{k\in C_\ell^-} M_k^c\,\underset{\sim}{\dot{u}}_k^{-1} + \frac{\Delta t}{2}\sum_{k\in C_\ell^-}\underset{\sim}{\tau}_k^{-1},\quad \ell\in\{1,2,\ldots,N^2\}$$

The subscripts 'left' and 'right' on the C_ℓ^-'s indicate the subsets of C_ℓ^- to the left and right of target node ℓ, respectively.

The second subscript on the entries of $\dot{U}$ and $\underset{\sim}{B}$ refer to the coordinate direction, e.g. $b_{\ell 2}$ is the z_2 - component of $\underset{\sim}{b}_\ell$.

An argument which employs dynamic force balances in place of impulse-momentum conditions yields relations for updated accelerations and contact

forces. The end results are summarized as follows:

• The updated accelerations of the target nodes $\ddot{\underset{\sim}{u}}_{\ell}^{+}$ are determined by solving

$$\underset{\sim}{A}\ \ddot{\underset{\sim}{U}} = \underset{\sim}{B}' \tag{I-8}$$

where

$$\ddot{\underset{\sim}{U}} = \begin{bmatrix} \ddot{u}_{11}^{+} & \ddot{u}_{12}^{+} \\ \ddot{u}_{21}^{+} & \ddot{u}_{22}^{+} \\ \cdot & \cdot \\ \cdot & \cdot \\ \cdot & \cdot \\ \ddot{u}_{N^2 1}^{+} & \ddot{u}_{N^2 2}^{+} \end{bmatrix} \qquad \underset{\sim}{B}' = \begin{bmatrix} b'_{11} & b'_{12} \\ b'_{21} & b'_{22} \\ \cdot & \cdot \\ \cdot & \cdot \\ \cdot & \cdot \\ b'_{N^2 1} & b'_{N^2 2} \end{bmatrix}$$

$$\underset{\sim}{b}'_{\ell} = M_{\ell}^{t}\ \ddot{\underset{\sim}{u}}_{\ell}^{-} + \sum_{k \in C_{\ell}^{-}} M_{k}^{c}\ \ddot{\underset{\sim}{u}}_{k}^{-} - \sum_{k \in C_{\ell}^{-1}} \underset{\sim}{\tau}_{k}^{-}$$

In the above definition of $\underset{\sim}{b}'_{\ell}$, the superscripts refer to the last iteration.

• The updated accelerations of the contactor nodes which are in contact with the target segment are given by linear interpolation, i.e.

$$\ddot{\underset{\sim}{u}}_{k}^{+} = (1-\alpha_k)\ \ddot{\underset{\sim}{u}}_{\ell}^{+} + \alpha_k\ \ddot{\underset{\sim}{u}}_{\ell+1}^{+}$$

• The updated accelerations of contactor nodes which have released from the target sometime during the time step are given by

$$\ddot{\underset{\sim}{u}}_{k}^{+} = \ddot{\underset{\sim}{u}}_{k}^{-} - \underset{\sim}{\tau}_{k}^{-} / M_{k}^{c} \tag{I-9}$$

• The updated contact forces associated with nodes which are in contact with the target are given by

$$\underset{\sim}{\tau}_k^+ = \underset{\sim}{\tau}_k^- + M_k^c \left(\ddot{\underset{\sim}{u}}_k^- - \ddot{\underset{\sim}{u}}_k^+\right). \qquad \text{(I-10)}$$

The solutions of the systems of equations (I-7) and (I-8) are accomplished most efficiently with an unsymmetric tridiagonal solver. The following is a FORTRAN subroutine to carry out this procedure. The matrix $\underset{\sim}{A}$ is stored by rows as a one-dimensional array.

```
      SUBROUTINE TRISOL (A,B,NEQ)
      DIMENSION A(1),B(NEQ,2)
C ... REDUCE EQUATIONS TO UPPER TRIANGULAR FORM
      NM = 3 * NEQ-2
      I = 2
      DO 100  N = 1, NM, 3
      IF (A(N). EQ. 0.0) GO TO 100
      AA = A(N+2)/A(N)
      A(N+3) = A(N+3) - A(N+1) * AA
      B(I,1) = B(I,1) - AA * B(I-1,1)
      B(I,2) = B(I,2) - AA * B(I-1,2)
  100 I = I + 1
C ... BACKSUBSTITUTE
      I = NEQ
  200 IF (A(NM). EQ.0.0)  GO TO 210
      B(I,1) = B(I,1)/A(NM)
      B(I,2) = B(I,2)/A(NM)
  210 I = I - 1
      IF (I.LE.0) RETURN
      NM = NM-3
      B(I,1) = B(I,1) - A(NM+1) * B(I+1, 1)
      B(I,2) = B(I,2) - A(NM+1) * B(I+1, 2)
      GO TO 200
      END
```

b. Sliding Contact Condition

The impact and release conditions for the sliding contact (frictionless) case are similar to the stick case, but only involve normal components. To describe the procedure employed, we will need to introduce some new terminology. Local boundary coordinates are normal (n) - tangential (s) coordinates attached to each target element boundary (see Fig. I-3). Pseudo-normal coordinates for an interior target node ℓ are normal ($\tilde{n}$) -

tangential ($\tilde{s}$) coordinates with respect to the line joining target nodes ℓ-1 and ℓ+1, whereas for target boundary nodes they are the same as the local boundary coordinates (see Fig. I-13). All computations of impact and release data are done with respect to the configuration determined by the last iteration within the time step.

The velocity update is achieved as follows:

Transform all $\dot{\underset{\sim}{u}}$'s and $\underset{\sim}{\tau}$'s appearing in (I-5) and (I-6) to pseudo-normal coordinates. Solve (I-7) where $\underset{\sim}{B}$ is replaced by the analogous N^2x1 vector of normal ($\tilde{n}$) components. $\dot{\underset{\sim}{U}}$ will then be the updated $\tilde{n}$-components of velocity of the target nodes. (The $\tilde{s}$ components are unaffected by this process.) Rotate the $\tilde{n}$, $\tilde{s}$-components into local boundary coordinates. Obtain the boundary normal (n) components of the contactor velocities by linear interpolation of the updated n-component target velocities. (The s-components are unaffected.) For nodes which have released, equation (I-6) is to be applied with the $\tilde{n}$-components.

Accelerations and contact forces are updated as follows:

Rotate the $\ddot{\underset{\sim}{u}}$'s and $\underset{\sim}{\tau}$'s appearing in the definition of $\underset{\sim}{B}'$, (I-9) and (I-10) into pseudo-normal coordinates. Solve (I-8) where $\underset{\sim}{B}'$ consists only of the $\tilde{n}$-components; $\ddot{\underset{\sim}{U}}$ will be the updated $\tilde{n}$-components of the target node accelerations.

The $\tilde{s}$-components are unaffected. Rotate the $\tilde{n}$, $\tilde{s}$-components into local boundary coordinates and linearly interpolate to determine $\ddot{u}_k^+$. The s-components are unaffected. Updated $\tilde{n}$-components of contactor nodes which have released are given by (I-9) with k replaced by $\tilde{n}$. Updated $\tilde{n}$-component of contact force are given by (I-10) with k replaced by $\tilde{n}$. As before, the contact force for released nodes is zero.

c. Frictional Contact Condition

The impact and release conditions for the frictional case are identical,

for the $\tilde{n}$-components, to the frictionless case. For the $\tilde{s}$-components some modifications are required. In the ensuing discussion we consider only the $\tilde{s}$-components. Again systems similar to (I-7) and (I-8) are constructed. Here, let C_ℓ^- denote the subset of nodes in contact which are not sliding at the last iteration of the time step, and let C_ℓ^{-1} indicate the released nodes (including sliding nodes). Then, in the updating of velocities, $\tilde{s}$-components of $\underset{\sim}{\tau}_k^{-1}$ should be replaced by the $\tilde{s}$-components of $\kappa(\underset{\sim}{\tau}_k^{-1} + \underset{\sim}{\tau}_k^-)$, where κ is a shear correction factor which can be adjusted to accurately capture shear wave phenomena. In the present work we assume for simplicity $\kappa = 1$. (These remarks pertain to equations (I-5) and (I-6).) The $\tilde{s}$-components of velocity for the nodes in C_ℓ^- are computed by linear interpolation.

The updating of the $\tilde{s}$-components of acceleration and contact force proceeds as follows:

Formulate the $\tilde{s}$-component of $\underset{\sim}{B}'$ using $\ddot{\underset{\sim}{u}}_{\tilde{S}}^-$ and $\underset{\sim}{\tau}_{\tilde{S}}^-$. Then $\ddot{\underset{\sim}{U}}$ will be the updated $\tilde{s}$-components of acceleration for the sticking nodes. Released node $\tilde{s}$-accelerations are given by (I-9), and non-sliding node updated $\tilde{s}$-contact forces are given by (I-7). For nodes which are sliding there is no update of $\tilde{s}$-components of $\ddot{\underset{\sim}{u}}$ and $\underset{\sim}{\tau}$.

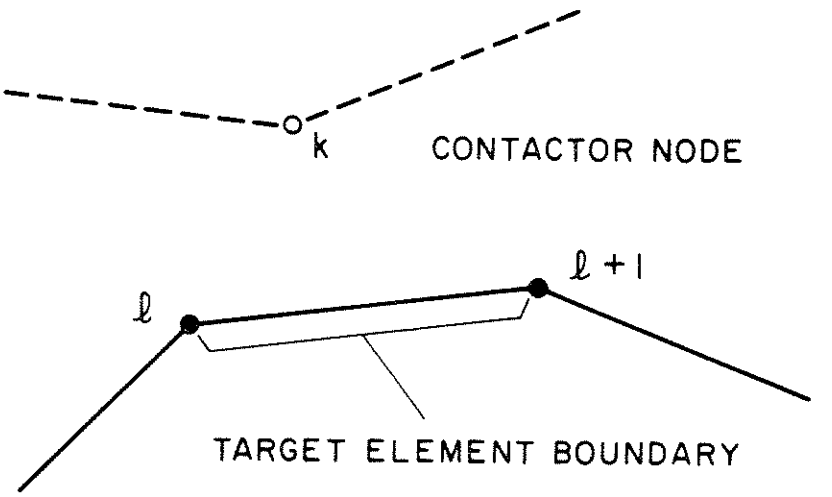

FIG. I-1 TYPICAL CONTACTOR NODE AND TARGET ELEMENT BOUNDARY

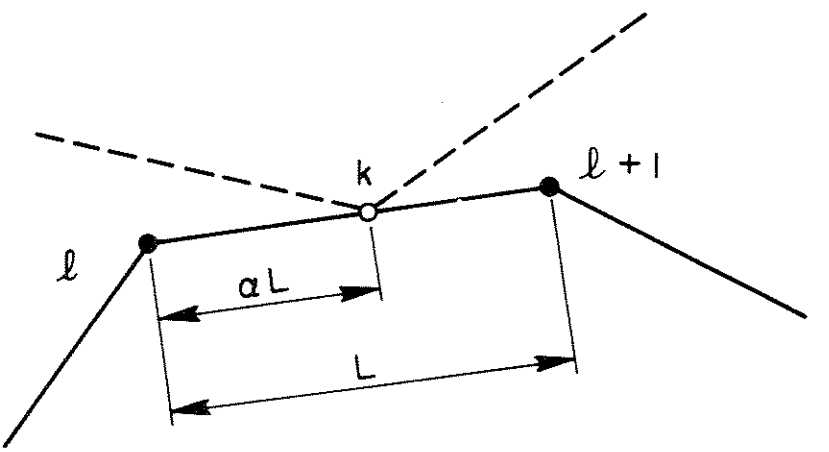

FIG. I-2 NONDIMENSIONAL LOCATION PARAMETER

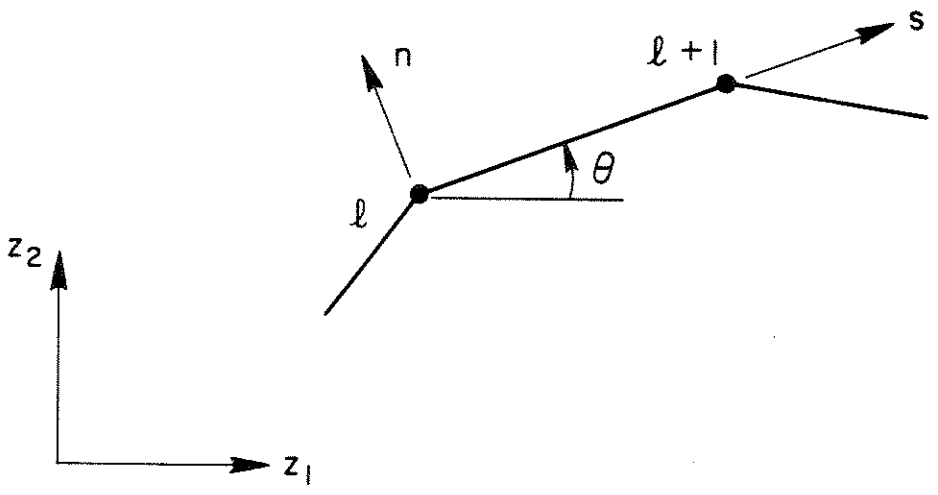

FIG. I-3 TARGET ELEMENT BOUNDARY LOCAL COORDINATE SYSTEM

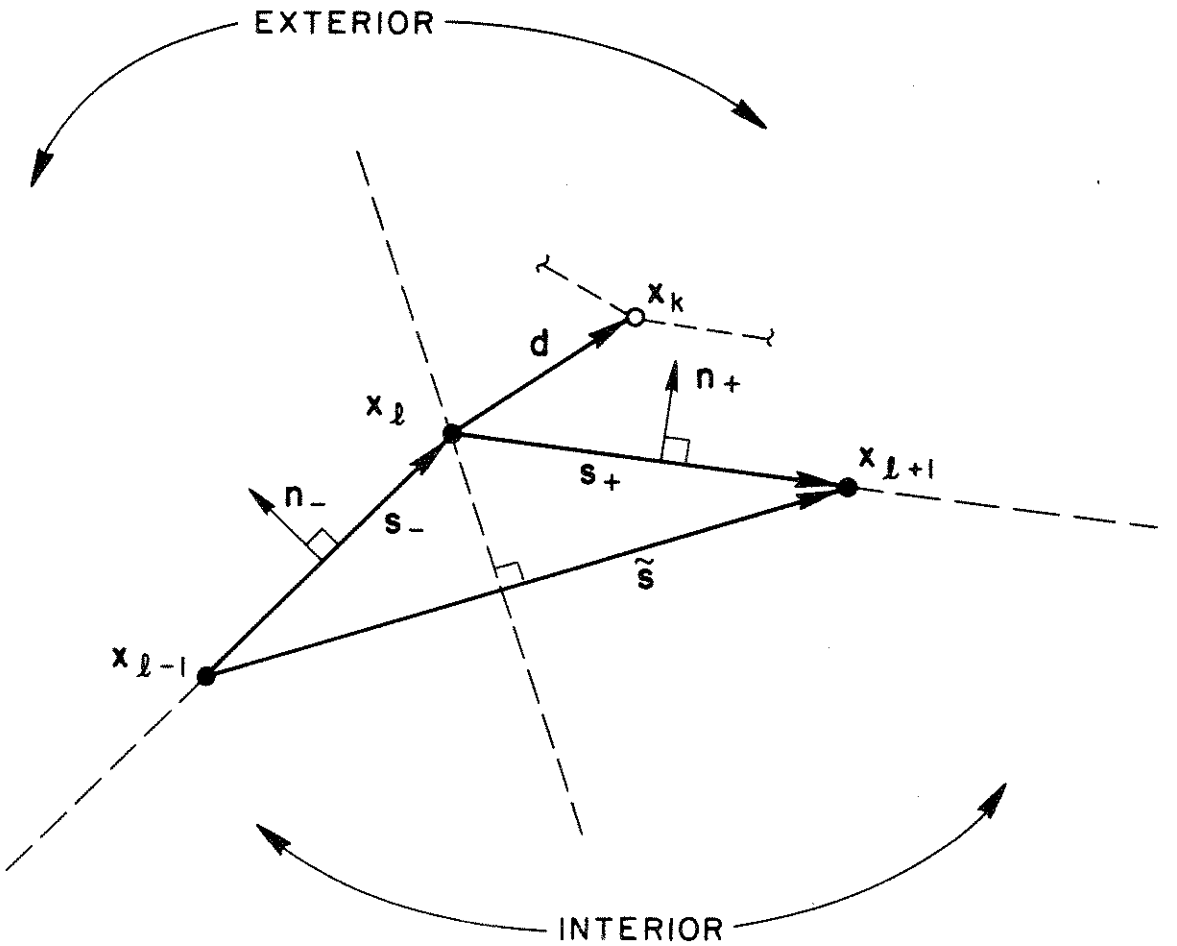

FIG. I-4 TYPICAL CONFIGURATION FOR CONTACTOR POINT $\underset{\sim}{x}_k$ AND TARGET SEGMENT REFERENCE POINT $\underset{\sim}{x}_\ell$

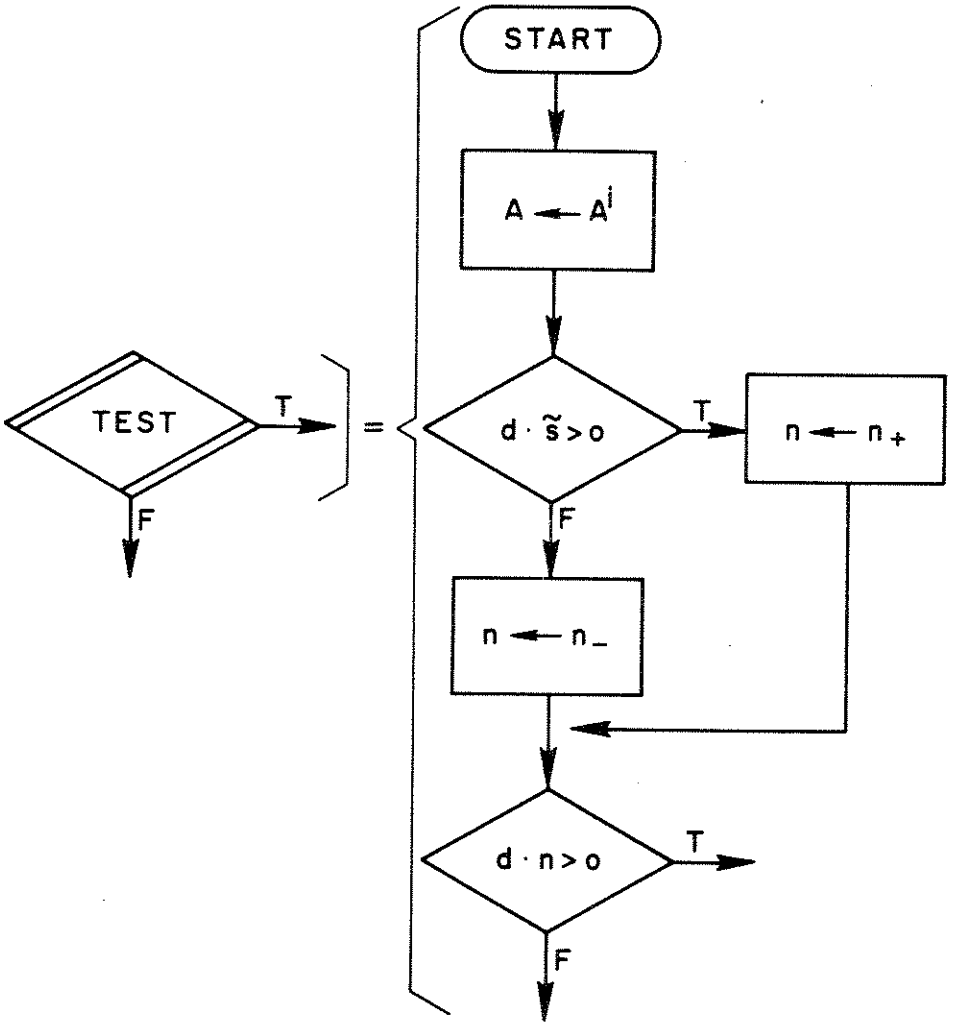

FIG. I-5 ALGORITHM TO DETERMINE IF A CONTACTOR NODE IS INTERIOR OR EXTERIOR TO THE TARGET

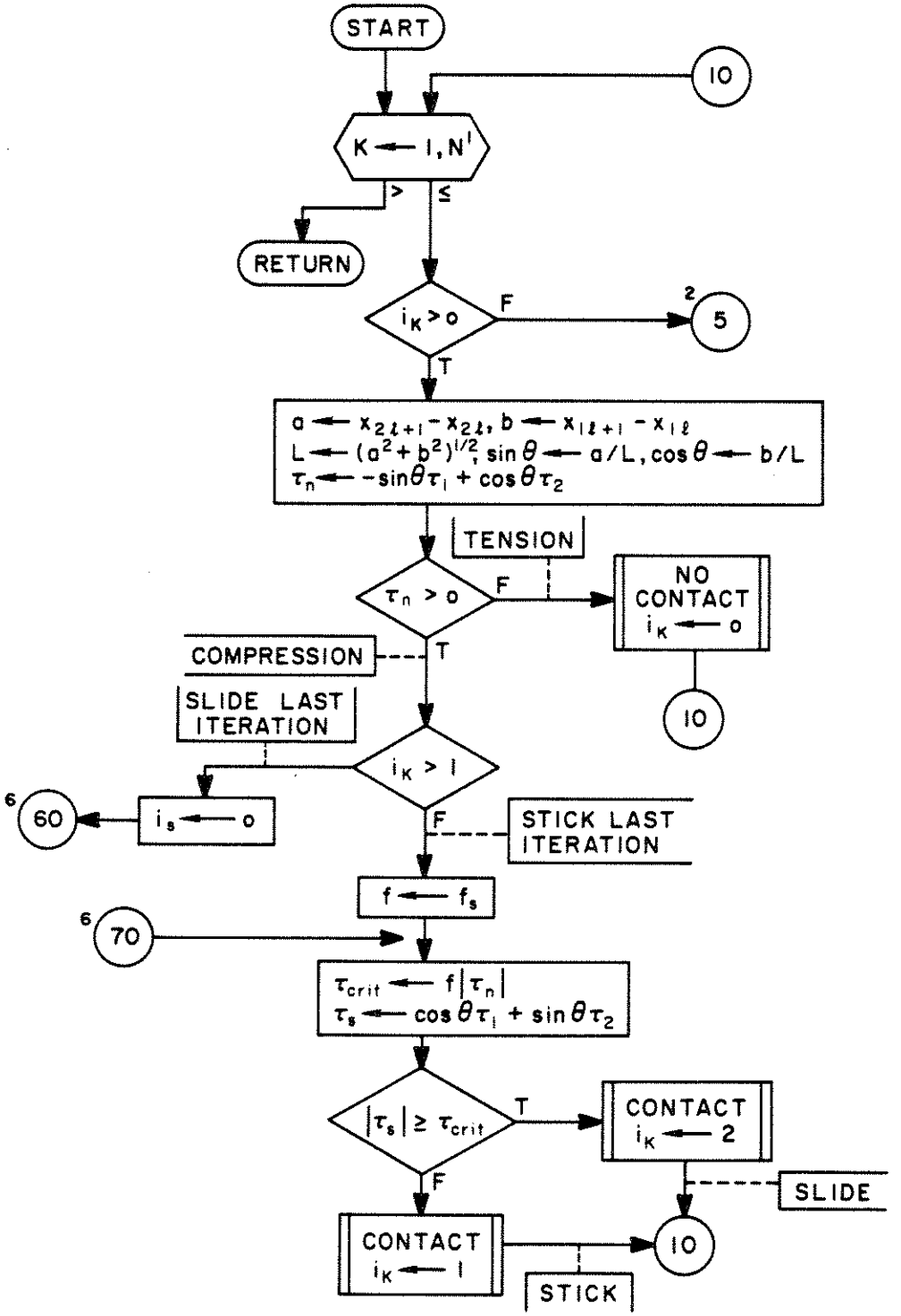

FIG. I-6 FLOW CHARTS WHICH DESCRIBE THE COMPUTING STRATEGY WITHIN A TIME (LOAD) STEP

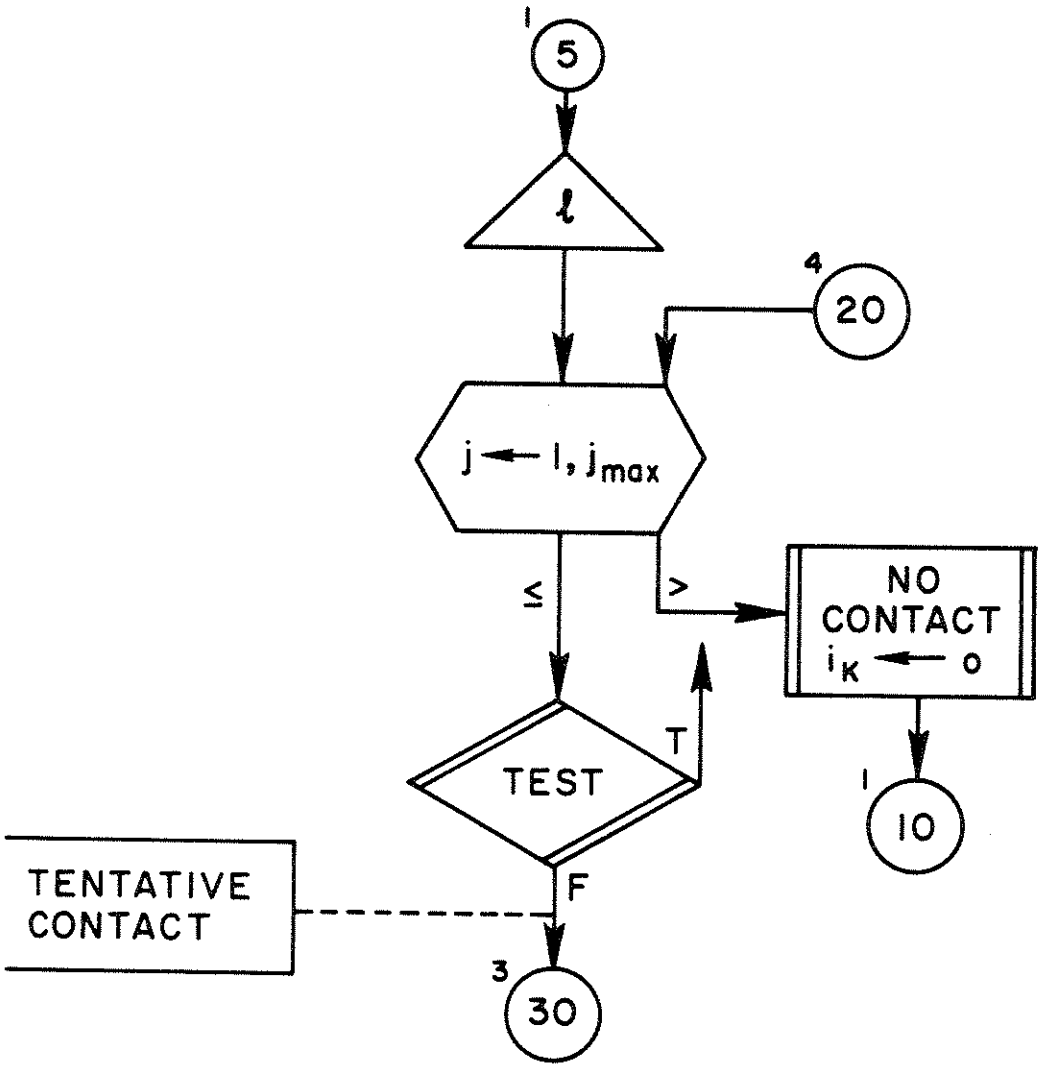
1
5
l
4
20
j ← l, j_max
≤
>
NO
CONTACT
i_K ← 0
T
TEST
1
10
TENTATIVE
CONTACT
F
3
30

FIG. I-7

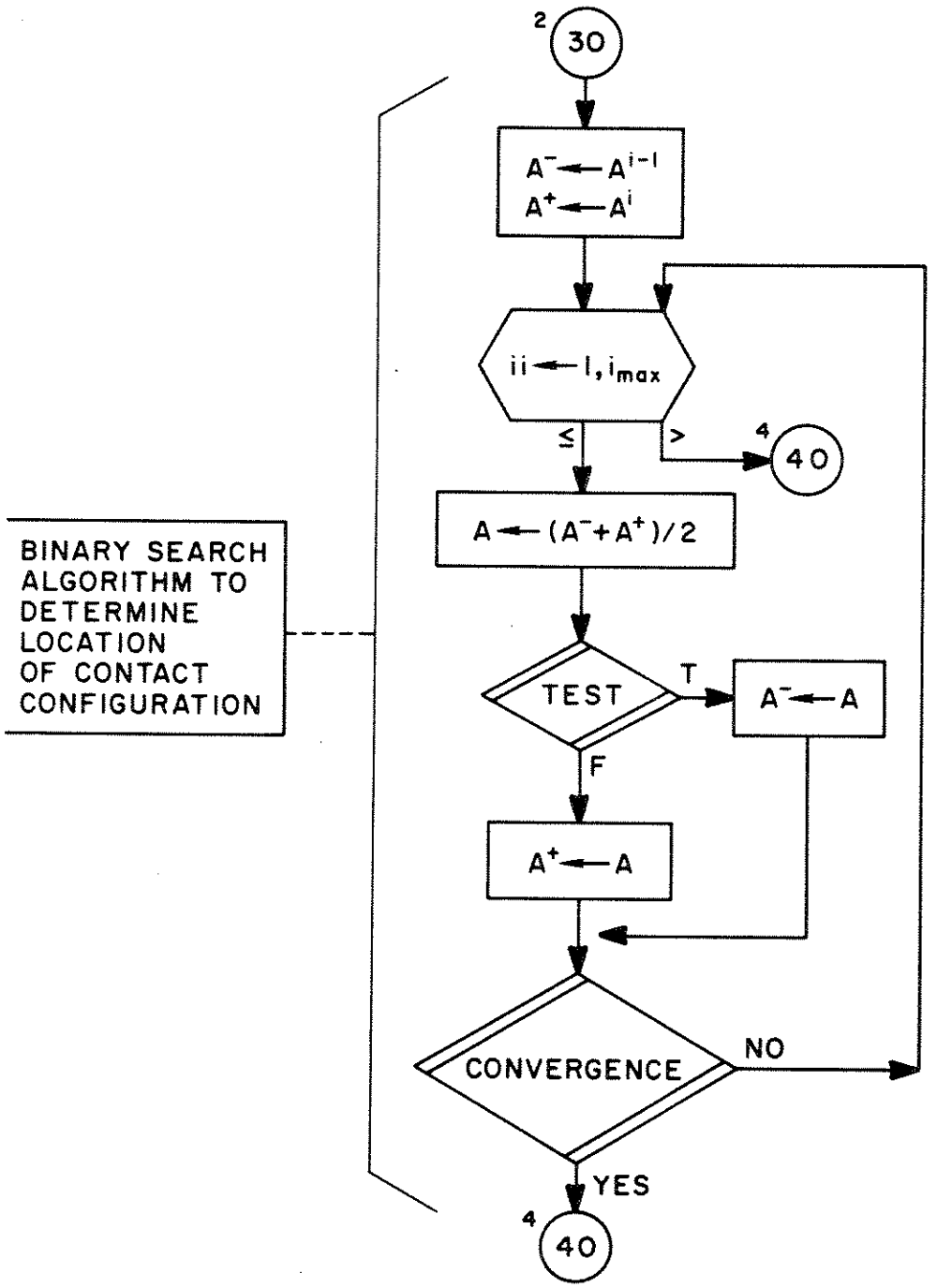
BINARY SEARCH ALGORITHM TO DETERMINE LOCATION OF CONTACT CONFIGURATION
2
30
A⁻ ← A^(i-1)
A⁺ ← A^i
ii ← 1, i_max
≤
>
4
40
A ← (A⁻+A⁺)/2
TEST
T
A⁻ ← A
F
A⁺ ← A
CONVERGENCE
NO
YES
4
40

FIG. I-8

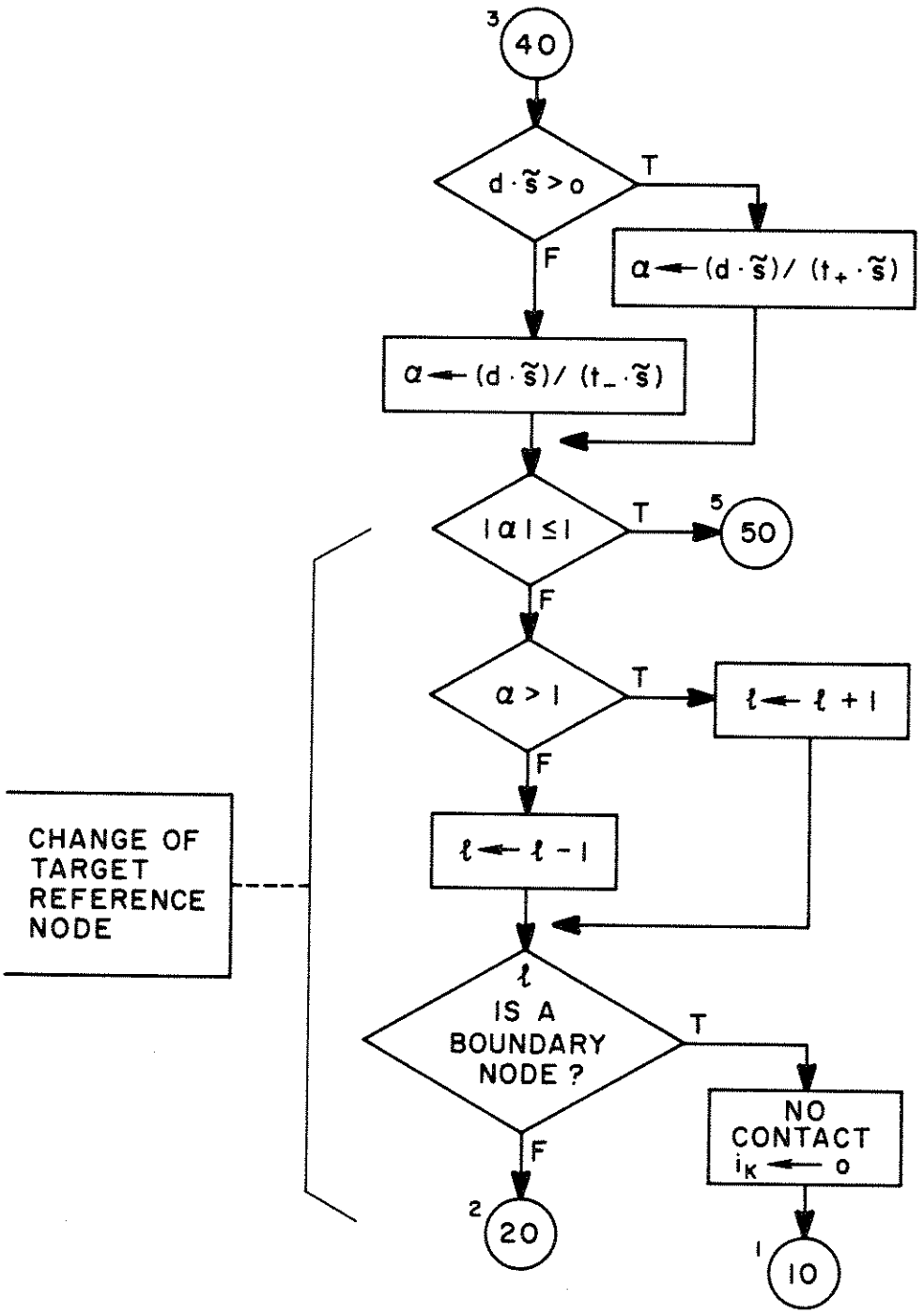
3
40
d · s̃ > o
T
F
α ← (d · s̃) / (t+ · s̃)
α ← (d · s̃) / (t− · s̃)
|α| ≤ 1
T
5
50
F
α > 1
T
ℓ ← ℓ + 1
F
ℓ ← ℓ − 1
CHANGE OF TARGET REFERENCE NODE
ℓ IS A BOUNDARY NODE ?
T
NO CONTACT
iK ← o
F
2
20
1
10

FIG. I-9

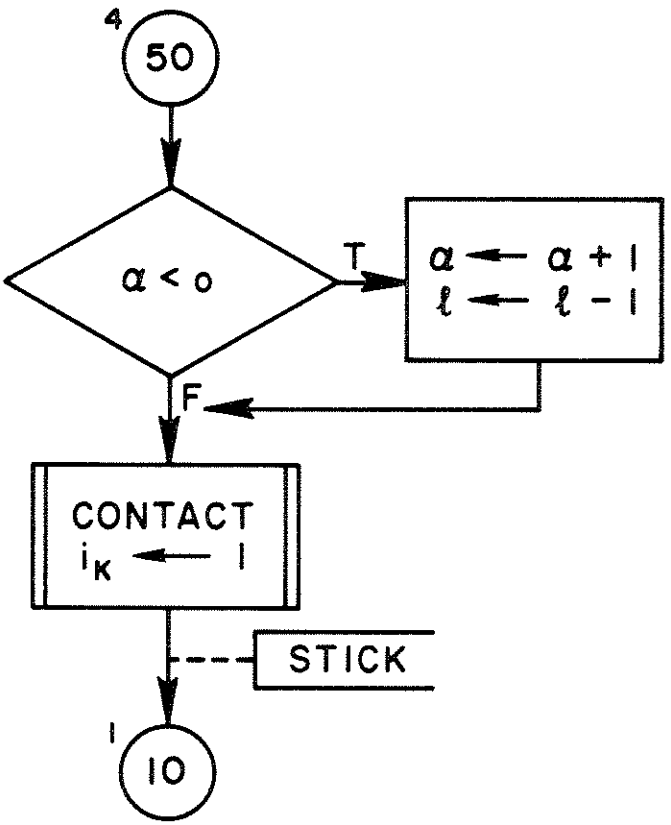

FIG. I-10

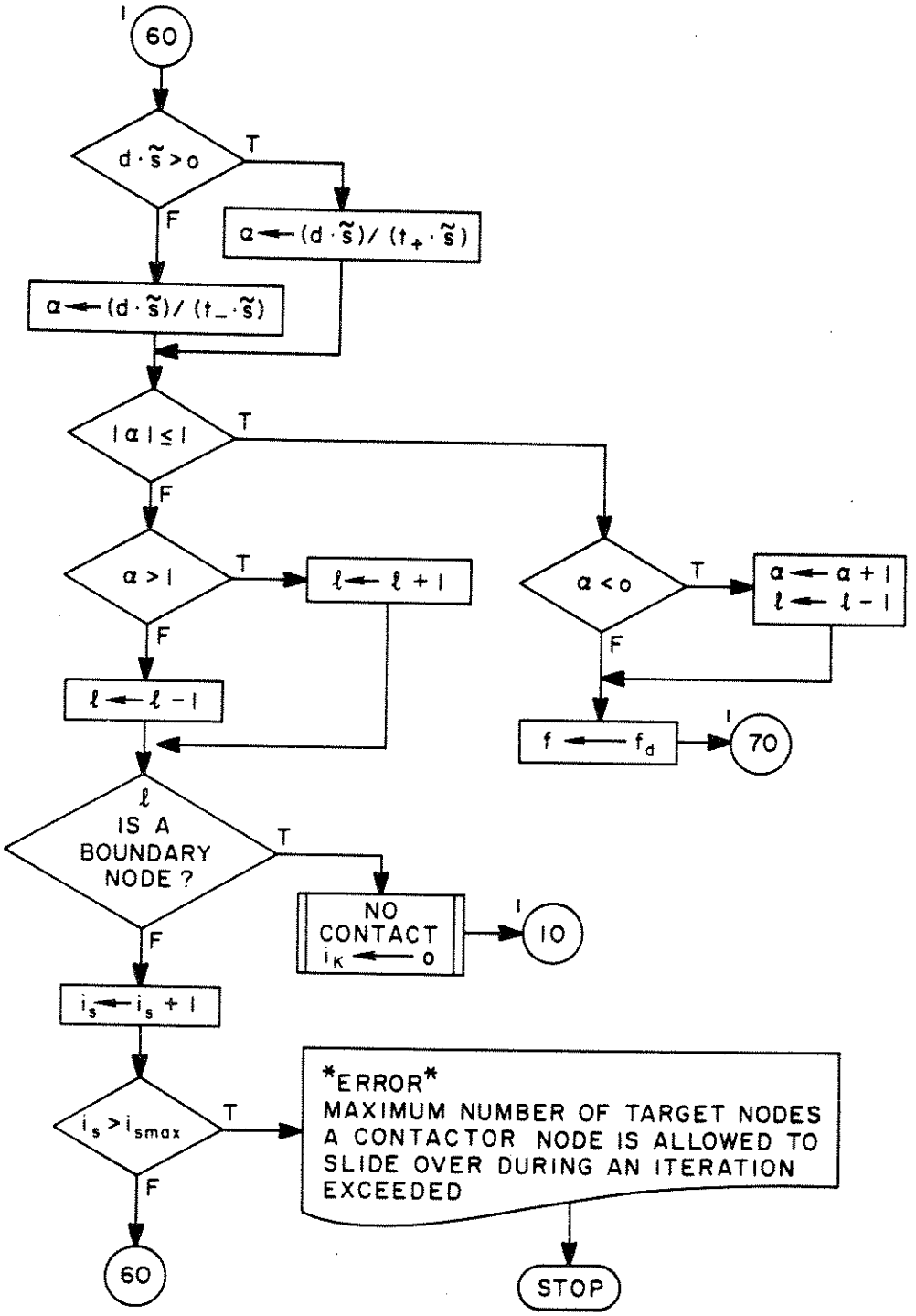
60
d · s̃ > o
T
F
α ← (d · s̃) / (t+ · s̃)
α ← (d · s̃) / (t− · s̃)
|α| ≤ 1
T
F
α > 1
T
ℓ ← ℓ + 1
F
ℓ ← ℓ − 1
α < o
T
α ← α + 1
ℓ ← ℓ − 1
F
f ← fd
70
ℓ
IS A BOUNDARY NODE ?
T
F
NO CONTACT
iK ← o
10
is ← is + 1
is > ismax
T
F
ERROR
MAXIMUM NUMBER OF TARGET NODES A CONTACTOR NODE IS ALLOWED TO SLIDE OVER DURING AN ITERATION EXCEEDED
60
STOP

FIG. I-11

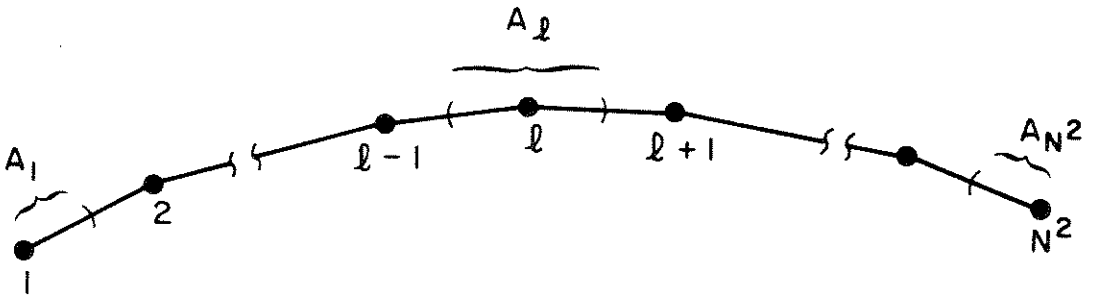

FIG. I-12 TRIBUTARY AREAS ASSOCIATED WITH TARGET NODES

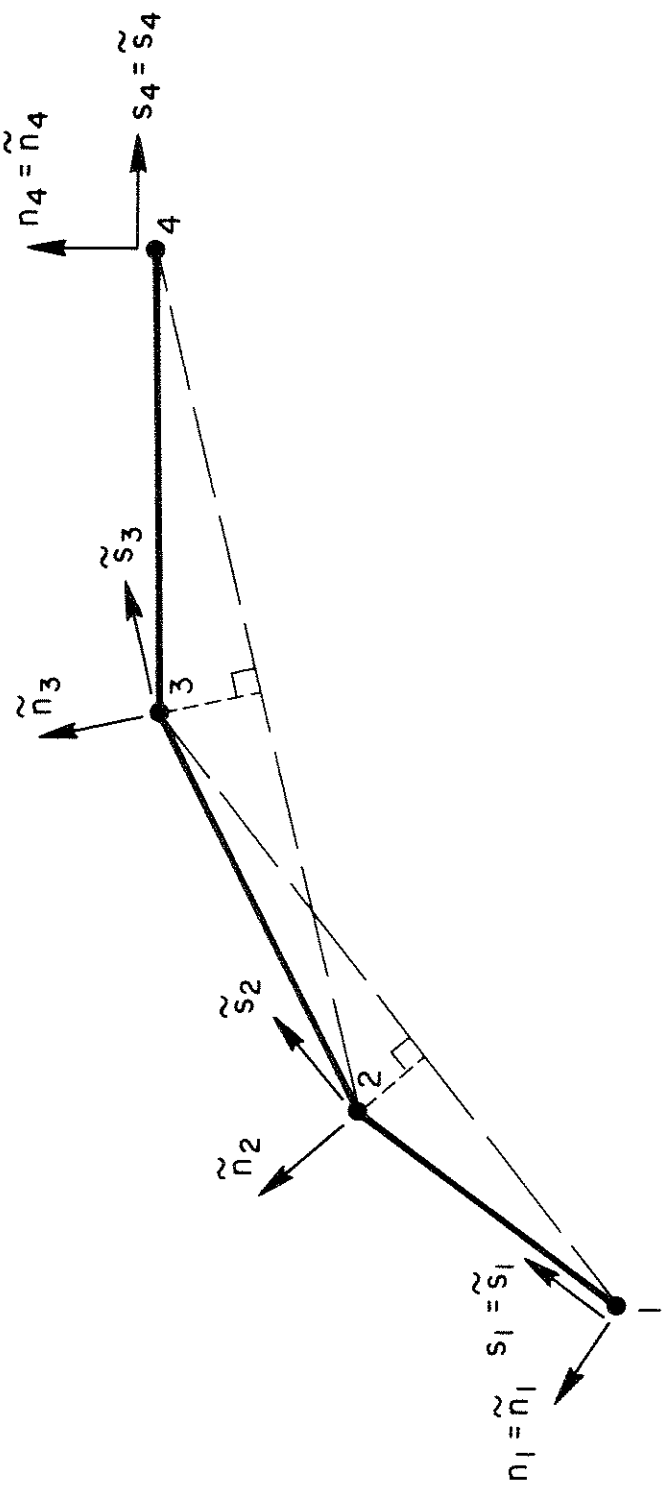

FIG. I-13 PSEUDO-NORMAL COORDINATES FOR AN OPEN TARGET SEGMENT CONSISTING OF FOUR NODES

II. New Developments with Particular Reference to the Hertzian Algorithm.

1. Introduction

In this chapter we describe some improvements to the Hertzian algorithm documented in our previous works; see [1-5].

2. Automatic Time Stepping

Often in impact problems the significant time scale during contact is much smaller than that when the bodies are not in contact. An example is illustrative. Consider the configuration of Fig. II-1. A simple frame structure, perhaps excited through ground motion, is vibrating in its fundamental mode. Let us take the period of the fundamental mode to be order 1. If in the course of the motion of the frame structure it impacts the rigid wall adjacent to it, perhaps representing a more massive structure, the characteristic time scale while in contact will be the transit time through the horizontal member. This could be orders of magnitude less than the period of the fundamental mode of the frame. To capture this phenomenon a very small time step would have to be taken compared with the period of the fundamental frame mode. On the other hand, a time step this small would be unnecessary and inefficient while the frame is not in contact.

To effectively accommodate situations such as the one just described an automatic time step feature has been programmed in FEAP. Three different time steps are read in as input data. The largest is employed if no contact is taking place. If contact occurs the intermediate time step is employed and the computation is repeated. The intermediate step is used subsequently until contact is again made at which time the computation is repeated with the smallest time step. The smallest time step is employed thereafter throughout the contact phase. If the bodies release the largest time step is again employed, and so on.

This feature should allow us to solve impact problems more economically in the future.

3. Higher-Order Impact-Release Conditions

In this section we shall describe higher-order impact and release conditions for the Hertzian algorithm. The necessity of developing a theory along these lines was first alluded to in [3], Section I-3-b, and subsequently in [4] and [5]. The theory is aimed at more accurately capturing the post-impact and post-release velocity states; the updated accelerations and tractions are computed as was done previously (see [4] or [5]). The reason for attempting to improve the velocity calculations is that no account is taken of the acceleration of the nodes in question. This can occasionally lead to poor results (see Section I-3-b of [3]). The theory presented herein accounts for acceleration and represents a negligible amount of additional computational effort.

We begin by quoting the discrete impact and release conditions for a typical pair of candidate contact nodes, presented in [4] and [5]:

impact

$$\dot{u}_+ = \frac{M^2\dot{u}_{-1}^2 + M^1\dot{u}_{-1}^1}{(M^1 + M^2)}$$

$$\ddot{u}_+ = \frac{M^1\ddot{u}_-^1 + M^2\ddot{u}_-^2}{(M^1 + M^2)}$$

$$\tau_+ = \tau_- - \frac{M^1 M^2}{(M^1 + M^2)}(\ddot{u}_-^2 - \ddot{u}_-^1)$$

release

$$\dot{u}_+^\alpha = \dot{u}_{-1} + (-1)^\alpha \Delta t\, \tau_{-1}/2M^\alpha$$

$$\ddot{u}_+^\alpha = \ddot{u}_-^\alpha - (-1)^\alpha \tau_- / M^\alpha$$

$$\tau_+^\alpha = 0$$

The notation is as follows: Superscripts refer to the body number and $\alpha = 1,2$. The subscript -1 indicates that the quantity in question is evaluated at the previous time step, the subscript - refers to the last iteration of the present time step, and the subscript + refers to the updated values accounting for impact-release effects. Arguments leading to these equations are presented in [1], [4] and [5]. The refinements to these quations to follow effect only the velocity equations. First we consider the case of impact.

It can be argued from wave-propagation theory that the updated velocity $\dot{u}_+$ is a good approximation to the velocity of the coalesced contact nodes at the instant following impact. If impact occurs towards the beginning of a time step, $\dot{u}_+$ may not be a very accurate representation for the end of the step. We seek to account for this effect in a rational way. To do this we make use of the fact that from the instant after impact to the end of the time step, the velocity is a reasonably smooth function. With this we define a new updated velocity

$$\dot{u}_{++} = \dot{u}_+ + \ddot{u}_+ \overline{\Delta t}$$

where $\overline{\Delta t} = t_{n+1} - t_c$, $t_c \in [t_n, t_{n+1}]$ is the instant of contact, and t_n and t_{n+1} denote the beginning and end of the time step, respectively. The picture is as illustrated in Fig. II-2. It remains to obtain an expression for $\overline{\Delta t}$. To do this, we approximate the position of the contact nodes in terms of the data from the previous time step, viz.

$$x^\alpha = X^\alpha + u_{-1}^\alpha + (\Delta t - \overline{\Delta t})\, \dot{u}_{-1}^\alpha + \frac{(\Delta t - \overline{\Delta t})^2}{2} \ddot{u}_{-1}^\alpha ,$$

where X^α denotes the initial position of the candidate contact mode of body α. The contact location is defined by

$$x^1 = x^2 ,$$

which leads to

$$\overline{\Delta t} = \Delta t - \frac{-b \pm (b^2 - 4ac)^{1/2}}{2a}$$

where

$$a = \ddot{u}_{-1}^{2} - \ddot{u}_{-1}^{1}$$

$$b = \dot{u}_{-1}^{2} - \dot{u}_{-1}^{1}$$

$$c = \chi^2 - \chi^1 + u_{-1}^{2} - u_{-1}^{1}$$

The physically relevant solution is determined by the condition

$$0 \leq \overline{\Delta t} \leq \Delta t$$

If no solution satisfies this condition $\overline{\Delta t}$ is set to $\Delta t/2$.

To obtain improved release velocities we also attempt to estimate a more accurate time of release within the step. Since the nodes were in contact at the end of the previous step, $\tau_{-1} > 0$. Let $\bar{\tau}$ denote the last value of contact force before release occurred. In keeping with our previous conventions (see [4] or [5]), $\bar{\tau}$ will be negative (indicating tension) or less than or equal to 2% of τ_{-1}. In the latter case we maintain the use of $\dot{u}_{+}^{\alpha}$ as the post-release velocity. (We note that the second term on the right-hand side of the expression for $\dot{u}_{+}^{\alpha}$ represents the impulse over the time step, assuming linear interpolation between τ_{-1} and zero.) In the case in which $\bar{\tau} < 0$, we compute (see Fig. II-3)

$$\overline{\Delta t} = \bar{\tau}/(\bar{\tau} - \tau_{-1}) .$$

The new updated velocity is then defined to be

$$\dot{u}_{++}^{\alpha} = \bar{\dot{u}}_{+}^{\alpha} + \ddot{u}_{+}^{\alpha} \overline{\Delta t}$$

where

$$\bar{\dot{u}}_{+}^{\alpha} = \dot{u}_{-1} + (-1)^{\alpha} (\Delta t - \overline{\Delta t}) \tau_{-1}/2M^{\alpha} \quad .$$

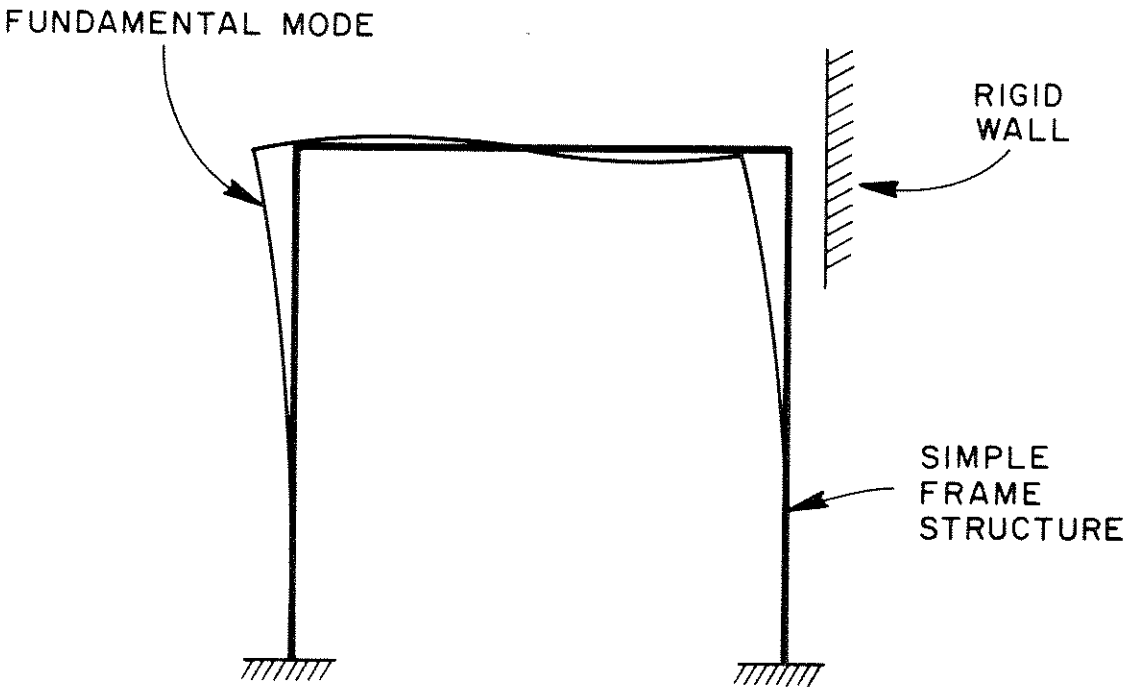

FIG. II-1 SIMPLE FRAME IMPACTING A RIGID WALL

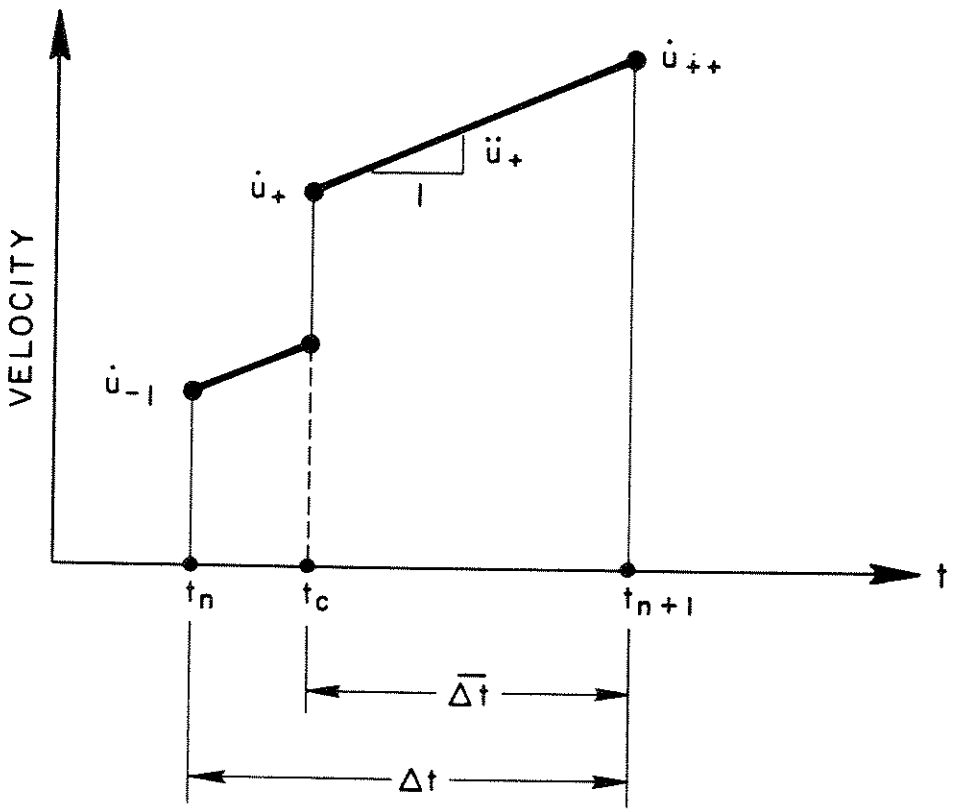

FIG. II-2 VELOCITIES BEFORE AND AFTER IMPACT

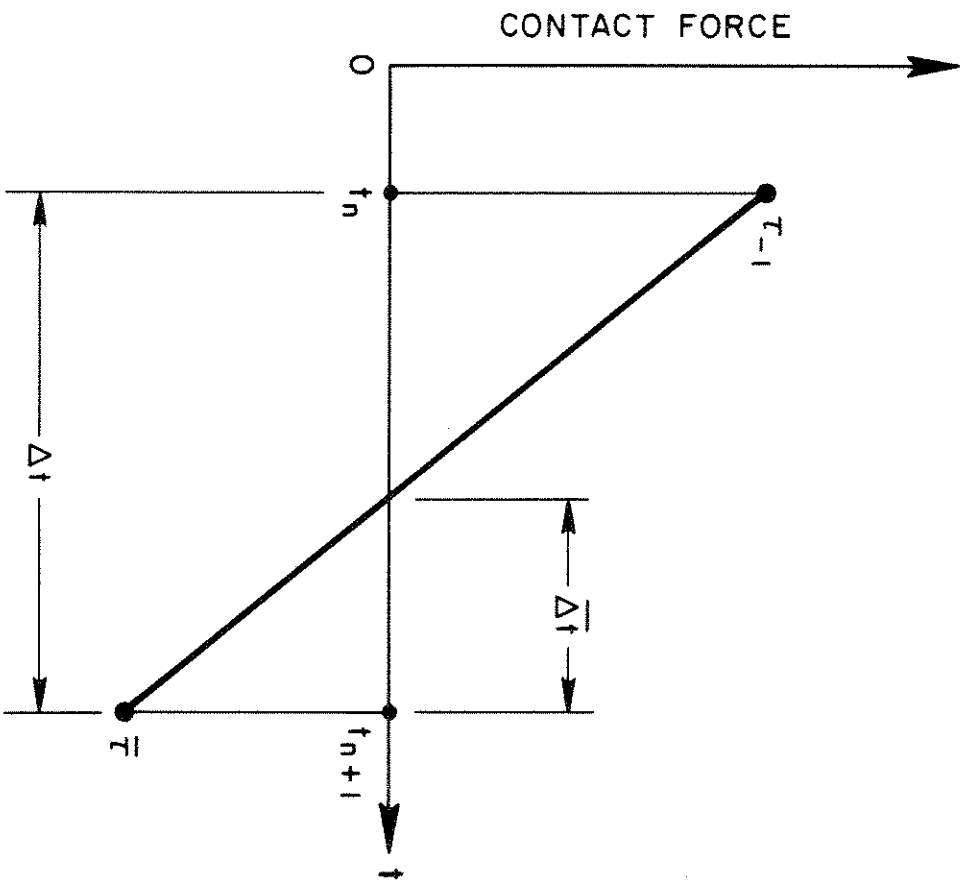

FIG. II-3 CONTACT FORCE BEFORE AND AFTER IMPACT

III. Sample Problem

1. Identification of Urethane-Polystyrene Composite Foam for the Nonlinear Continuum Element.

The theory for a nonlinear elastic continuum element was presented in [3], Sections II-2 and II-3. This element has been programmed in FEAP and the following options are available:

2-D { plane strain, plane stress, axisymmetric

3-D

Two different quadrature rules can be employed in each case: 2 x 2 Gaussian quadrature for all terms, or 2 x 2 Gaussian quadrature for μ-terms and 1-point quadrature for λ-terms (see [3] for notation and further details). The latter option is appropriate for incompressible and nearly-incompressible applications. For use in subsequent check problems, we have selected the parameters λ and μ so that a close fit is obtained to the loading cycle for a urethane-polystyrene composite foam described in [6]. Values of $E = 50$ psi and $\nu = .1, .25, .3$ were selected which, for the configuration illustrated in Fig. III-1, leads to the response illustrated in Fig. III-2. As can be seen, the best results are obtained with $\nu = .25$. In subsequent calculations, unless otherwise indicated, $E = 50$ psi and $\nu = .25$ were employed.

2. Equivalence of Present Incompressible Formulation with a Mean-Pressure-Variable Element.

In [3], on p. 32, we conjectured that employing 2 x 2 Gaussian quadrature on the μ-terms, and 1-point quadrature on the λ-terms, for the standard four-node isoparametric quadrilateral, might yield results identical to the constant mean pressure-bilinear displacement element employed in the past by Hughes and Allik [7]. We have attempted to corroborate this conjecture by performing an analysis using both elements. Consider the configuration illustrated in Fig. III-3. The beam is modelled with plane strain rectangular using several different quadrature rules and the constant mean pressure-bilinear displacement element of [7]. The beam is fixed at the left end and a uniform shear is applied to the right end. The results confirm the equivalence of the 'underintegrated' element with the constant mean pressure-bilinear displacement element.

We thank H. Allik and P. Caccistore of the Electric Boat Division of General Dynamics, Groton, Connecticut, for providing us with the results for the constant mean pressure-bilinear displacement element. (Recently an analytical study has been performed which establishes the equivalence of the two elements; see Hughes [8].)

3. Quasi-Static Analysis of a Skull-Pad Contact Configuration

This analysis consists of a cylindrical 'skull' model being contacted with a soft pad. The material properties of the three-layer skull are those quoted in [3], Table I-1*, and originally obtained from [9]. The pad material is that described in Section III-1. Linear elements are used to model the skull and nonlinear elements are used to model the pad. All elements employ the plane strain option and 2 x 2 Gaussian quadrature. The skull is fixed at the uppermost node and the pad is driven into the skull and withdrawn by way of prescribing a uniform displacement condition along the bottom of the pad. The initial gap between skull and pad is 0.1inches. The maximum vertical displacement of the bottom of the pad is 0.5inches and the displacement is applied in steps of 0.1inches. Unloading is performed similarly. The contact condition is assumed to be perfect friction along the contact surface. Thus there is no tangential slipping while in contact. Release occurs when tension is sensed normal to the target segment (in this case the pad). The analysis employs the 'between node' contact element described in [2], Section II-3, and the kinematically nonlinear search algorithm described in [3], Section III. The target segment consists of the seven element boundaries along the top surface of the pad. There is a total of seven contactor nodes -- the innermost seven nodes along the bottom outer surface of the skull. Initial and deformed configurations are depicted in Fig. III-4. The unloading steps are identical to the loading steps (i.e. step numbers 6-4, 7=3, 8=2, 9=1, 10=0) and thus not shown. Note that the contactor nodes contact the target segment between nodes.

* There is a typographical error in the table. The density of the brain material should be $.937 \times 10^{-4}$ lb-sec^2/in^4. This was the value actually used in the analyses.

The strain in the pad elements near the axis of symmetry reach a maximum strain of approximately 50% and the pad elements near the periphery of the contact zone experience a maximum rotation of approximately 30°. Normal and tangential contact stresses, at the point of maximum contact area development, are plotted in Fig. III-5. The pad has the effect of more uniformly distributing the contact force than a rigid surface; cf. [3], Section I-1-a. Total vertical contact force and contact area width are plotted, versus applied displacement step number, in Fig. III-6.

In our initial attempts to solve this problem we observed a lack of convergence. This was due to the following situation: Nodes frequently released and then recontacted during iterating within a step. The point of contact was set to the last penetration point, rather than the initial contact point. This was in violation of the stipulated no-slip condition. In addition, the contactor node along the symmetry axis penetrated the contact surface without contact being sensed. This was due to a small negative horizontal displacement, caused by round-off, which made the search algorithm think the contactor node was outside the target segment. Upon correcting these fallibilities convergence was achieved.

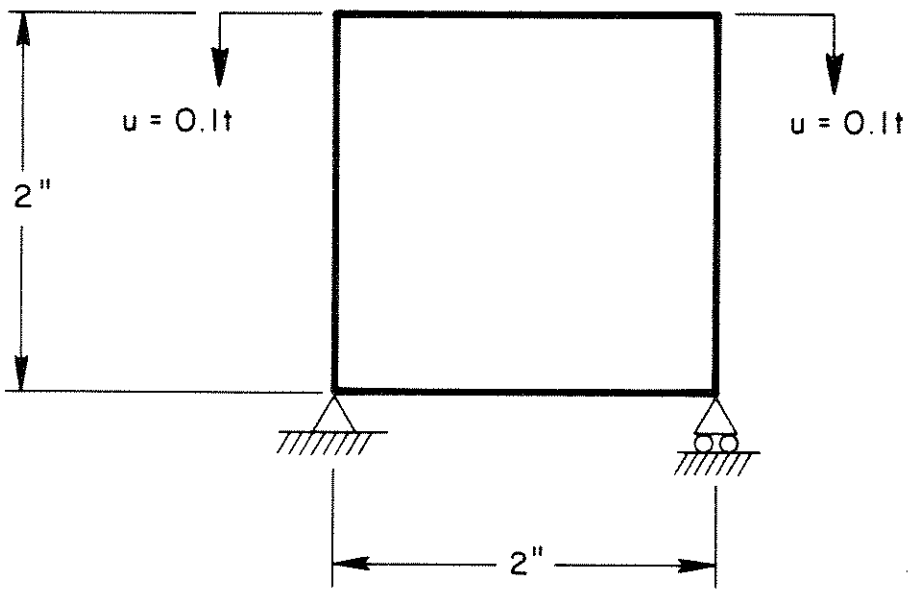

FIG. III-1 ONE 3D CONTINUUM ELEMENT WITH A UNIFORM COMPRESSIVE DISPLACEMENT ALONG THE TOP SURFACE FOR IDENTIFICATION OF URETHANE-POLYSTYRENE COMPOSITE FOAM

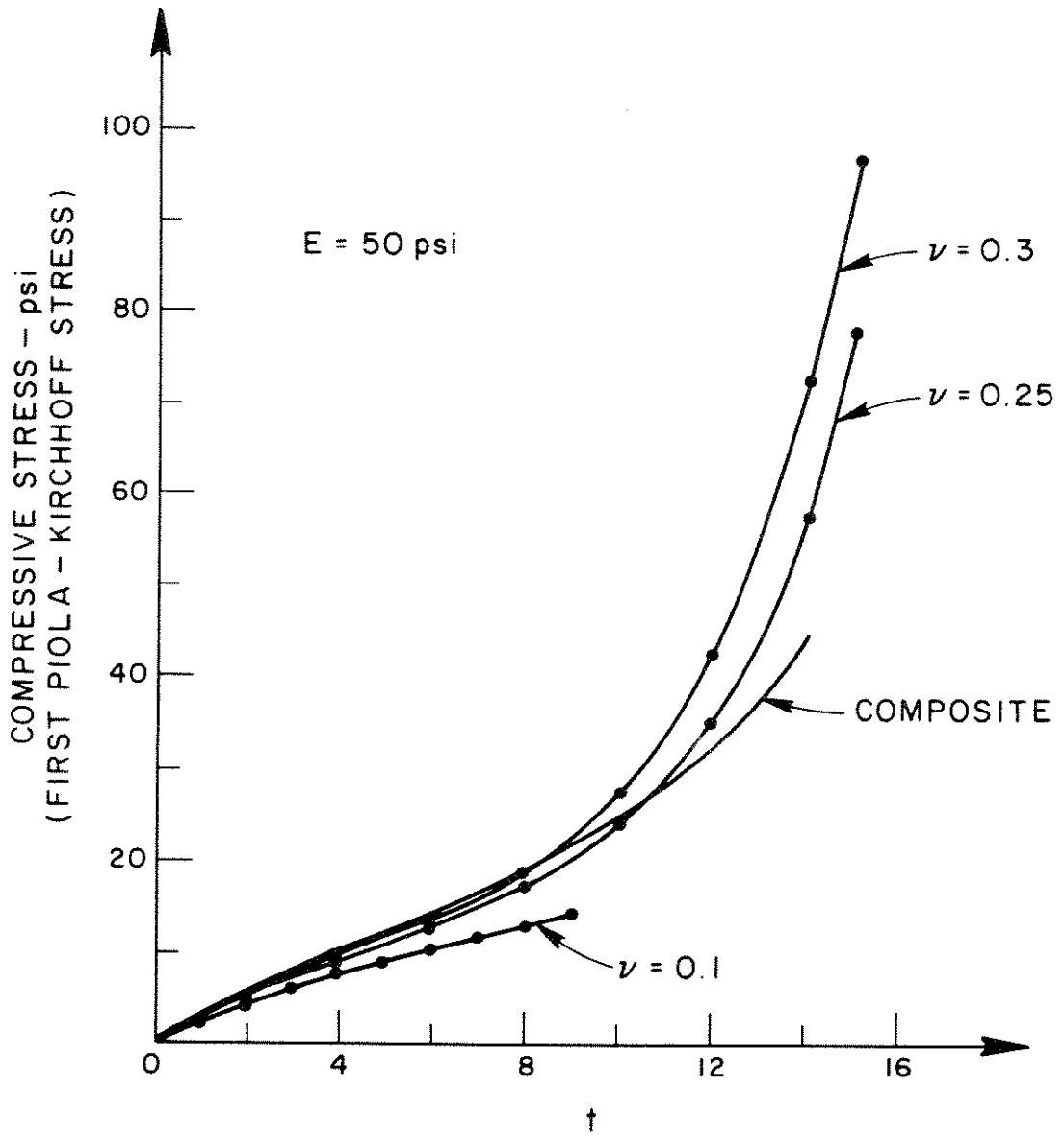

FIG. III-2 RESPONSE OF UNIFORMLY COMPRESSED CONTINUUM ELEMENT COMPARED WITH RESPONSE OF URETHANE-POLYSTYRENE COMPOSITE FOAM

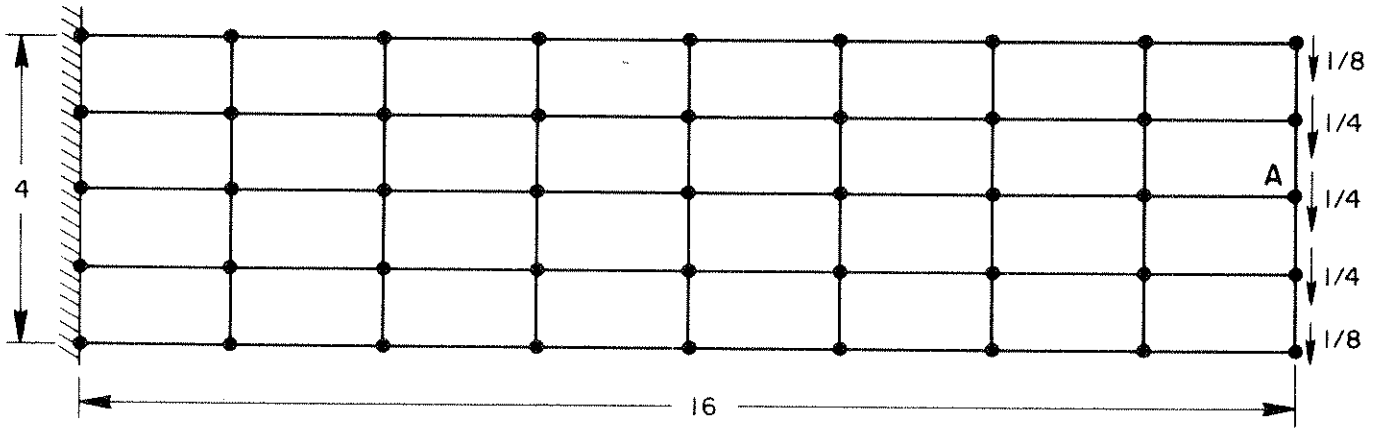

VERTICAL DISPLACEMENT AT POINT A , E=1

ELEMENT	QUADRATURE	$\nu = 0.3$	$\nu = 0.499$
BILINEAR DISPLACEMENTS	EXACT	217.8	26.8
BILINEAR DISPLACEMENTS	$1 \times 1 - \lambda$ TERM $2 \times 2 - \mu$ TERM	224.9	183.3
CONSTANT PRESSURE - BILINEAR DISPLACEMENTS	EXACT	224.9	183.3
BILINEAR DISPLACEMENTS	$1 \times 1 - \lambda + 2\mu/3$ TERM $2 \times 2 - \mu$ TERM	228.3	186.9

FIG. III-3 COMPARISON OF NUMERICALLY INTEGRATED QUADRILATERALS WITH CONSTANT PRESSURE-BILINEAR DISPLACEMENT ELEMENT

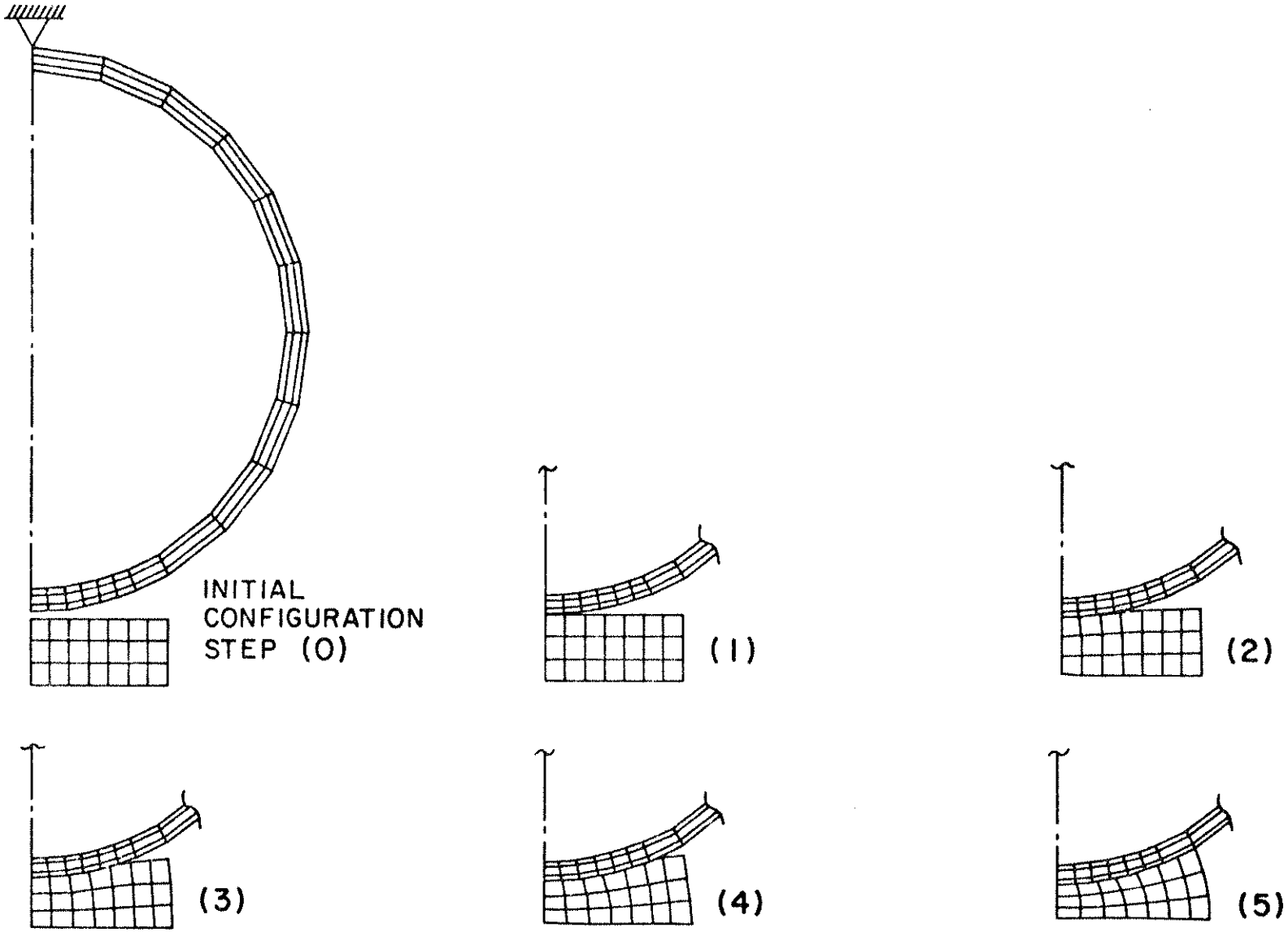

FIG. III-4 INITIAL (0) AND DEFORMED (1-5) MESH CONFIGURATIONS FOR A CYLINDRICAL SHELL CONTACTING A SOFT NONLINEAR PAD

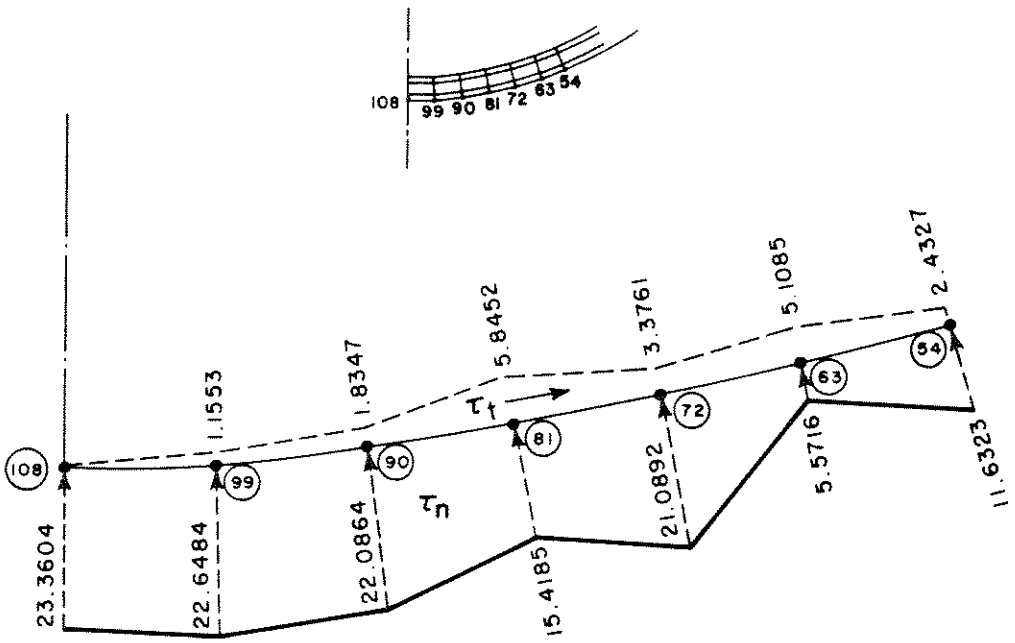

FIG. III-5 NORMAL AND TANGENTIAL CONTACT STRESSES (PSI) FOR CYLINDRICAL SHELL CONTACTING A SOFT NONLINEAR PAD

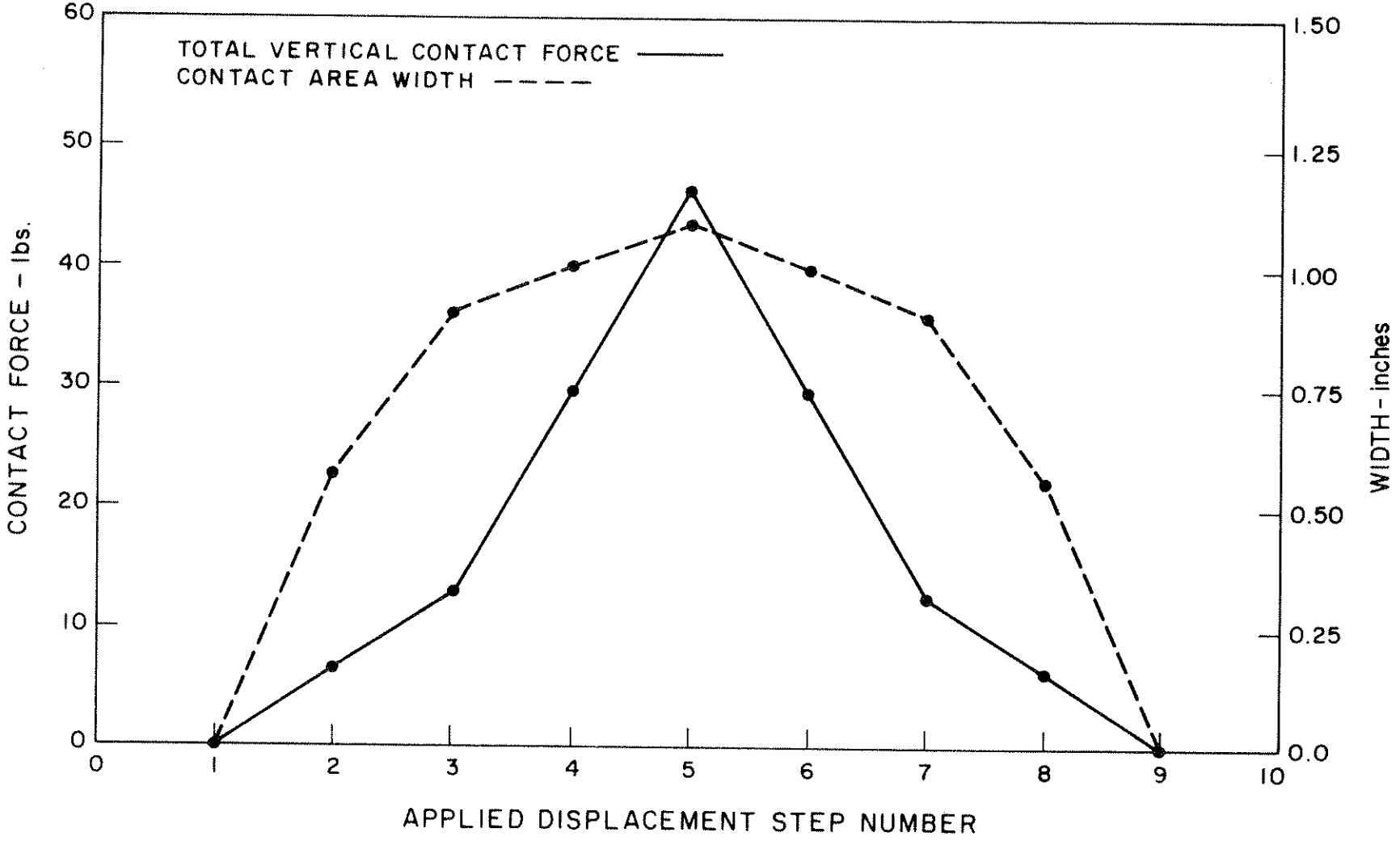

FIG. III-6 CONTACT FORCE AND CONTACT AREA WIDTH VERSUS APPLIED DISPLACEMENT

IV. A Simple and Efficient Finite Element for Plate Bending

1. Introduction

An enormous amount of effort has been devoted to the development of finite elements for the bending of plates. The literature is extensive and we will not make an attempt to review it here. (The interested reader may consult any of the standard texts for references, e.g. [10-12].) Most of this effort has been oriented towards linear problems; in particular, to the classical Poisson - Kirchhoff theory of bending. The C^1-continuity requirement imposed by this theory on 'displacement' finite element models precludes the development of simple and natural elements (see [13]). Because of this, incompatible elements (e.g. [14-15]) are often resorted to, since they involve simpler programming than the rather complicated C^1-continuous elements (e.g. [15-17]) and are competitive from an accuracy standpoint.

Accurate higher-order C^1-elements have also been developed (e.g. [18-20]), but they too are quite complicated and involve nodal derivative degrees-of-freedom of order greater than one, which complicates the specification of boundary conditions.

The assumed stress hybrid bending elements of Pian and his associates (e.g. [21]) have proven to be accurate, but they have some drawbacks and thus are not widely used.

Another approach to the development of bending elements for thin plates involves the so-called 'discrete Kirchhoff hypothesis' (e.g. [22,23]). In this approach the classical equations are abandoned in favor of a bending theory which includes shear deformations. The result is that only C^0-continuity is required of the shape functions. To capture the behavior of thin plate theory, the constraint of zero shear

strains is imposed at a discrete number of points. The method is effective, but implementations tends to be somewhat complicated. Recent improvements and variants on this theme have been proposed by Fried [24-26].

An accurate quadrilateral element for thick and thin plates has been developed by Zienkiewicz, Taylor and Too [27]. This element possesses eight nodes--four corner and four midside--with the basic three degrees-of-freedom per node. The transverse displacement and rotation shape functions are selected from the 'serendipity' family (see [10]). Two-by-two Gaussian quadrature is an essential requirement for the good performance of the element.

In summarizing these developments one can confidently assert that for linear problems of plate bending many adequate elements exist. The choice is more a matter of taste as no single element is clearly superior to the rest in all cases.

Many users of finite element computer programs find a 'basic' four-node quadrilateral element particularly appealing due to its simplicity. It is our feeling that this appeal will become even greater when nonlinear applications are undertaken. In the nonlinear regime--and especially in nonlinear dynamics--computational cost is the prime concern. Due to frequent reformulations of tangent stiffnesses, complicated element routines can lead to exorbitant computational expenditures and may actually preclude nonlinear analysis. A simpler element of competitive accuracy becomes quite desirable under such circumstances. Other factors in nonlinear analysis buttress this assertion. For example, the accuracy level attainable in nonlinear problems is often severely limited due to the uncertainty of nonlinear material characterizations. Thus it makes little sense to engender significant computational cost for complicated

bending elements which are only marginally more accurate than simpler elements, since the confidence level of the overall analysis may be affected only negligibly. Unfortunately, heretofore, no really simple alternative has existed.

In this chapter we attempt to remedy this situation. We develop what we believe is the simplest effective plate bending element yet proposed. The element is a four-node quadrilateral with the basic three degrees-of-freedom per node. The element shape functions are bilinear for transverse displacement and rotations. The shear 'locking' associated with such low-order functions in application to thin plates is eleviated by splitting the shear and bending energies and using one-point quadrature on the shear term. The simplicity of the element lends itself to concise and efficient computer implementation.

To develop the theory in its simplest setting, we consider in Section IV-2 a beam element involving linear displacement and rotation shape functions. We show how exact integration (two-point Gaussian quadrature) of the element stiffness matrix leads to an overly stiff element and we present an heuristic argument why this is the case. We then show how employing one-point quadrature on the shear term lessens the stiffness. The concept is identical for the plate bending element which is developed in Section IV-3. The effectiveness of the element in thin plate bending is demonstrated in Section IV-4. A simple computing strategy for dealing with the numerically sensitive case of extremely thin plates is presented in Section IV-5. In Section IV-6 we consider applications to thick plates. It is shown that the element is still effective for moderately thick plates. However, for very thick plates, in which the thickness of individual elements exceed their characteristic lengths, a slight modification of the shear quadrature need be employed.

2. Example: Linear Beam Element

In this section we will describe the formulation of a beam element stiffness for which displacement and rotation are assumed to be independent linear functions. Exact integration of the element stiffness can be facilitated by two-point Gaussian quadrature, whereas one-point integration exactly integrates the bending contribution, but 'underintegrates' the shear contribution. For the case of thin beams we view the shear term as a constraint which attempts to enforce the condition of negligible shear strains. We shall show that one-point quadrature has a decisively positive effect on the accuracy of the element; two-point quadrature leading to worthless numerical results. The upshot of all this is that by appropriately underintegrating troublesome terms, good bending behavior can be attained by the simplest shape functions.

The equations of a rectangular cross-section beam, including shear deformation effects, emanate from the following expression for strain energy:

$$U(w,\theta) = \frac{1}{2}\frac{Et^3}{12}\left[\int_0^L \left(\frac{d\theta}{dx}\right)^2 dx + \kappa \frac{12G}{Et^2} \int_0^L \left(\frac{dw}{dx} - \theta\right)^2 dx\right], \qquad \text{(IV-1)}$$

where w is the transverse displacement of the center-line, θ is the rotation of the cross-section, E is Young's modulus, G is the shear modulus, κ is the shear correction factor (throughout we employ $\kappa = 5/6$), t is the depth, L is the length and x is the axial coordinate. The first term on the right-hand side of (IV-1) is the bending energy and the second is the shear energy. With independent expansions for w and θ, (IV-1) can be employed to derive beam element stiffness matrices. The case we are interested in is when both w and θ are assumed to behave linearly over an element. This leads to a four-degree-of-freedom element

in which displacement and rotation are the nodal degrees-of-freedom. By virtue of the fact $d\theta/dx$ is constant within this element, the bending energy may be exactly evaluated by one-point Gaussian quadrature. On the other hand, two-point Gaussian quadrature is required to exactly integrate the shear energy term due to the explicit presence of θ, which is linear within the element. Employing one-point quadrature on the shear energy term 'underintegrates' the element and it is our prime concern here to ascertain the effect of this procedure. (See also Gallagher [11], pp. 364-367.)

A series of test computations were performed to determine the behavior of the element. A cantilever beam subjected to an end load (see Fig. IV-1) was analyzed for various discretizations. The first example is for a relatively deep beam. The data are:

$$E = 1000$$
$$G = 375$$
$$t = 1$$
$$L = 4$$

Tip displacement results for several discretizations are presented in Table IV-1. As is evident, the one-point quadrature results are vastly superior to the two-point results. A more severe test for linear elements is bending governed by Bernoulli - Euler theory. In this case shear strains are to be equal to zero. Such a situation can be brought about in the present theory if depth is taken very small compared with element length. Alternatively, a very large fictitious value of G can be specified. In the second example we attempt to ascertain the behavior of the linear element when the assumptions of the Bernoulli - Euler theory apply. The data of the previous example are employed with the

Table IV-1. Normalized tip displacement for a deep cantilever beam.

Number of elements	Tip displacement-- one-point quadrature	Tip displacement-- two-point quadrature
1	.762	$.416 \times 10^{-1}$
2	.940	.445
4	.985	.762
8	.996	.927
16	.999	.981

Table IV-2. Normalized tip displacement for a thin cantilever beam.

Number of elements	Tip displacement-- one-point quadrature	Tip displacement-- two-point quadrature
1	.750	$.200 \times 10^{-4}$
2	.938	$.800 \times 10^{-4}$
4	.984	$.320 \times 10^{-3}$
8	.996	$.128 \times 10^{-3}$
16	.999	$.512 \times 10^{-3}$

exception of G which is set here to 375×10^5. Results are listed in Table IV-2. The one-point quadrature results are quite accurate whereas the two-point results are in error by approximately three orders of magnitude. Early attempts at developing bending elements with simple shape functions were abandoned because of results like those for the two-point quadrature presented here.

We shall now proceed to give a heuristic argument why two-point quadrature causes such an overly stiff element. Consider a cantilever beam discretized into N elements. In the assembled stiffness matrix there are 2N degrees-of-freedom -- two degrees-of-freedom per element. The shear contribution to the stiffness represents a constraint on the shear strains. If one-point quadrature is employed, one constraint is imposed upon the element, whereas if two-point quadrature is employed, two constraints are imposed upon the element. In the latter case the number of constraints per element equals the number of degrees-of-freedom per element, and the result is that the mesh 'locks'.

This can be seen more precisely by looking at the stiffness contributions of the bending and shear terms. We assume the nodal degrees of freedom are ordered as follows: w_1, θ_1, w_2, θ_2; and h is the element length. The stiffnesses are:

$$k_b = \frac{Et^3}{12h} \begin{bmatrix} 0 & 0 & 0 & 0 \\ 0 & 1 & 0 & -1 \\ 0 & 0 & 0 & 0 \\ 0 & -1 & 0 & 1 \end{bmatrix} \qquad \text{(IV-2a)}$$

$$k_s^{(1)} = \frac{\kappa G t}{h} \begin{bmatrix} 1 & h/2 & -1 & h/2 \\ h/2 & h^2/4 & -h/2 & h^2/4 \\ -1 & -h/2 & 1 & -h/2 \\ h/2 & h^2/4 & -h/2 & h^2/4 \end{bmatrix} \qquad \text{(IV-2b)}$$

$$k_s^{(2)} = \frac{\kappa G t}{h} \begin{bmatrix} 1 & h/2 & -1 & h/2 \\ h/2 & h^2/3 & -h/2 & h^2/6 \\ -1 & -h/2 & 1 & -h/2 \\ h/2 & h^2/6 & -h/2 & h^2/3 \end{bmatrix} \qquad \text{(IV-2c)}$$

where k_b is the bending stiffness, and $k_s^{(1)}$ and $k_s^{(2)}$ are the one-point and two-point quadrature shear stiffnesses, respectively. It is easily verified that the rank of $k_s^{(1)}$ is one and the rank of $k_s^{(2)}$ is two. In the latter case, k_b is completely dominated by the shear stiffness, as the following simple example illustrates.

Consider the case of a one-element cantilever beam, subjected to an end load P and moment M.

(i) <u>One-point quadrature</u>.

Combining (IV-2a) and (IV-2b), eliminating appropriate rows and columns, and solving for the tip displacement and rotation yields

$$w = (h^2/4\alpha + \beta^{-1})\, P + hM/2\alpha \ , \qquad \text{(IV-3a)}$$

$$\theta = (hP/2 + M)/\alpha \ , \qquad \text{(IV-3b)}$$

where

$$\alpha = Et^3/12h, \tag{IV-3c}$$

$$\beta = \kappa Gt/h. \tag{IV-3d}$$

In the thin beam limit (i.e., when $\beta >> \alpha$), (IV-3a) becomes

$$w = h(hP/2 + M)/2\alpha, \tag{IV-4}$$

and (IV-3b) remains unchanged. Thus we are left solely with the deformation due to bending as is right.

(ii) Two-point quadrature.

Carrying out the same steps as in case i, with (IV-2c) in place of (IV-2b), yields

$$w = \left(\frac{\alpha + h^2\beta/3}{\beta\ \gamma}\right) P + hM/2\gamma, \tag{IV-5a}$$

$$\theta = (hP/2 + M)/\gamma, \tag{IV-5b}$$

where

$$\gamma = \alpha + h^2\beta/12. \tag{IV-5c}$$

In the thin beam limit (IV-5a) and (IV-5b) become

$$w = (4P + 6M/h)/\beta, \tag{IV-6a}$$

$$\theta = 6(hP + 2M)/h^2\beta, \tag{IV-6b}$$

respectively. In this case only deformations due to shear are in evidence and (IV-6a) and (IV-6b) are $O(t^{-2})$ in error.

In passing we note that there are some circumstances in which the present element may have some practical value. For example, an axisymmetric shell version might be useful for shell covered solids in which bilinear elements are used to model the solid. The fact that only one

quadrature point is involved may lead to more economical computations in nonlinear analysis.

3. Bilinear Plate Bending Element

The strain energy for an isotropic, linearly elastic plate, including shear deformation, is

$$U(w, \theta_1, \theta_2) =$$

$$\frac{Et^3}{24(1-\nu^2)}\left\{ \iint_A \left[\left(\frac{\partial \theta_1}{\partial x_1}\right)^2 + 2\nu \frac{\partial \theta_1}{\partial x_1}\frac{\partial \theta_2}{\partial x_2} + \left(\frac{\partial \theta_2}{\partial x_2}\right)^2 + \frac{(1-\nu)}{2}\left(\frac{\partial \theta_1}{\partial x_2} + \frac{\partial \theta_2}{\partial x_1}\right)^2 \right] dx_1\, dx_2 \right.$$

$$\left. + \frac{6\kappa(1-\nu)}{t^2} \iint_A \left[\left(\frac{\partial w}{\partial x_1} - \theta_1\right)^2 + \left(\frac{\partial w}{\partial x_2} - \theta_2\right)^2 \right] dx_1\, dx_2 \right\} , \qquad \text{(IV-7)}$$

where x_1 and x_2 are cartesian coordinates, w is the transverse displacement, θ_1 and θ_2 are the rotations about the x_1 and x_2 axes, respectively, E is Young's modulus, ν is Poisson's ratio, κ is the shear correction factor, t is the plate thickness and A is its area. The first integral in (IV-7) represents the bending energy and the second represents the shear energy. We consider a four-node quadrilateral element and assume the displacement and rotations are expanded in independent bilinear shape functions. The isoparametric concept is employed (see Zienkiewicz [10]). This results in three degrees-of-freedom -- one displacement and two rotations -- at each of the corners.

For very thick plates two-by-two Gaussian quadrature leads to acceptable results, however, for thin plates it causes 'locking' as indicated for the beam in the previous section. In this case we use two-by-two Gaussian quadrature on the bending energy term and one-point Gaussian quadrature on the shear energy term. This results in one constraint per element. In large meshes there are approximately three equations per element, thus there is no danger of the mesh 'locking'.

As is apparant, the proposed element is extremely simple, and easily and concisely coded. We are certain that the element routines are faster than any other plate bending element yet proposed. In the next section we will show that the element is also surprisingly accurate.

4. Numerical Examples: Thin Plates

In this section we present several numerical examples which have become more or less standard ones for evaluating plate elements. All computations were performed on a CDC 6400 computer in single precision. (A single precision word consists of 60 bits on the CDC 6400.)

Square Plate

The data for this example consists of the following (see Fig. IV-2):

$$E = 10.92 \times 10^5$$

$$\nu = .3$$

$$t = .1$$

$$L = 10$$

Both simply supported and clamped boundary conditions were considered as well as concentrated and uniformly distributed loadings. Results are presented in Tables IV-3 and IV-4 for κ values of 1000 and 5/6. The former value is set to artificially maintain the Poisson-Kirchhoff constraint. Due to the fact that the plate is rather thin ($L/t = 100$), there is little difference in the results for the two values of κ. In fact, the bending moments are identical. In practical situations there seems no point in exceeding the 'natural' value of $\kappa = 5/6$.

Moment and shear resultants, and displacements are plotted in Fig. IV-3 along the line $x_1 = 0$, for the clamped, concentrated load case in which $\kappa = 5/6$. Along $x_1 = 0$ and $x_2 = 0$, the x_1 and x_2 components of the moment are equal, as are the x_1 and x_2 components of the shear.

The simply supported concentrated load case has, it seems, taken on the role of the preeminent comparison problem for bending elements. In Fig. IV-4 the present element, with $\kappa = 1000$, is compared with data taken from Gallagher [11]. The good convergence of the element is evident.

Clamped Circular Plate

The data for this example is the same as for the previous problem except (see Fig. IV-5):

$$R = 5$$

$$t = .1$$

Results are presented in Table IV-5 for concentrated and uniform loadings, and κ values of 1000 and 5/6.

Again, due to the thinness of the plate, there is little difference in the displacement results for the two values of κ, and the moment results are identical.

Table IV-3. Normalized center displacement and bending moment for a simply supported square plate.

Number of elements	Displacement-- Concentrated load	Displacement-- Uniform load	Moment-- Uniform load
4	.9922	.9770	.851
16	.9948	.9947	.963
64	.9982	.9987	.991

(a) $\kappa = 1000$

Number of element	Displacement-- Concentrated load	Displacement-- Uniform load	Moment-- Uniform load
4	.9957	.9782	.851
16	.9991	.9960	.963
64	1.0034	.9997	.991

(b) $\kappa = 5/6$

Table IV-4. Normalized center displacement and bending moment for a clamped square plate.

Number of elements	Displacement-- Concentrated load	Displacement-- Uniform load	Moment-- Uniform load
4	.8652	.9535	.822
16	.9650	.9850	.955
24	.9920	.9937	.986

(a) $\kappa = 1000$

Number of elements	Displacement-- Concentrated load	Displacement-- Uniform load	Moment-- Uniform load
4	.8720	.9575	.822
16	.9748	.9890	.955
64	1.0034	.9976	.986

(b) $\kappa = 5/6$

Table IV-5. Normalized center displacement and bending moment for a clamped circular plate.

Number of elements	Displacement-- Concentrated load	Displacement-- Uniform load	Moment-- Uniform load
3	.9197	.8587	.827
12	.9579	.9535	.957
48	.9883	.9888	.990

(a) $\kappa = 1000$

Number of elements	Displacement-- Concentrated load	Displacement-- Uniform load	Moment-- Uniform load
3	.9267	.8621	.827
12	.9674	.9570	.957
48	1.0005	.9925	.990

(b) $\kappa = 5/6$

5. Numerical Sensitivity due to Extreme Thinness

The results of the previous section indicate that despite the simplicity of the present element it is quite accurate. However, one precaution must be taken when employing elements derived from the reduced integration concept. This admonition stems from the observation that the shear stiffness is $O((h/t)^2)$ times the bending stiffness. (In the case of a quadrilateral bending element h may be taken to be the length of the longest side.) For fixed h, as $t \to 0$, it is only a matter of time before the effect of the bending stiffness vanishes completely due to the finite computer word length. Results of this kind can be seen for the beam element in Fig. IV-6 and for the plate element in Fig. IV-7. The plateaus represent the appropriate solutions for the meshes in question in the 'thin' limit. Deterioration of the numerical solution begins to occur at $L/t = 10^4$ in the case of the beam, and $L/t = 10^5$ for the plate; this corresponds to element aspect ratios (i.e., h/t) of $10^4/16$ and $10^5/8$, respectively. It is unlikely that aspect ratios larger than these values will be met in practice. However, on computers with shorter single precision word length, deterioration will commence at smaller aspect ratios. Here it is important to employ a strategy which circumvents these difficulties. This can be done as follows: Determine the maximum element aspect ratio for which good results are obtained by plotting graphs similar to Figs. IV-6 and IV-7. Before combining the shear and bending contributions of the element stiffness test the aspect ratio. If it is less than the value for which good results are obtained, combine in the usual way. Otherwise, multiply the shear stiffness by $(t/h)^2$ times the square of the maximum element aspect ratio allowed, then combine. This will reduce the disparity between the bending and

shear term to an acceptable level, yet maintain thin element behavior. Numerical results illustrating these ideas are depicted in Figs. IV-6 and IV-7. The maximum allowable aspect ratios were determined to be $10^4/16$ for the beam element and $10^5/8$ for the plate element, from Figs. IV-6 and IV-7, respectively. Employing these values in the procedure described above enables the plateaus to be extended to the higher aspect ratios, as illustrated in Figs. IV-6 and IV-7. This process enables the reduced integration procedure to be applied successfully in cases involving arbitrarily large aspect ratios.

Of course, another way to avoid difficulties is to work in double precision on short word computers.

6. Application to Thick Plates

One-point Gaussian quadrature on the shear term has a decidedly beneficial effect in application to thin plates. However, the opposite is true for very thick plates. The difficulties do not always manifest themselves. For example, results for the uniformly loaded clamped circular plate are acceptable (see Fig. IV-8; q refers to the magnitude of the load). For t/R = .4 the results are of about the same level of accuracy as those in [27], where a higher-order element is employed. On the other hand, results for the same plate subjected to a concentrated load tend to oscillate about the exact solution (see Fig. IV-9). This problem is a trying one as the exact Reissner's theory solution consists of an infinite displacement under the load, viz.

$$w = \frac{PR^2}{16\pi D}\left[\underbrace{\left(1 - \frac{r^2}{R^2}\right) - \frac{2r^2}{R^2}\ln\frac{R}{r}}_{\text{bending}} - \underbrace{\frac{8D}{KGtR^2}\ln\frac{r}{R}}_{\text{shear}}\right]$$

$$\beta = \frac{PR}{4\pi D}\left[\frac{r}{R}\ln\frac{R}{r}\right]$$

where P is the concentrated force and D is the bending rigidity. As the plate thickness is reduced the oscillations are lessened (see Figs. IV-10 to IV-15). From these results we conclude that when the t/h ratio exceeds unity, the one-point Gaussian quadrature of the shear term should be abandoned in favor of the following scheme: Two-by-two Gaussian quadrature should be used on the $(\partial w/\partial x_1)^2$ and $(\partial w/\partial x_2)^2$ contributions to the shear energy. The remaining terms in the shear energy should be integrated as usual by one-point Gaussian quadrature. We refer to this element as the 'modified' one-point shear element.

A spectral analysis of the element stiffness, when one-point Gaussian quadrature is employed on the shear term, reveals that there are five zero eigenvalues -- two more than the usual three rigid body modes. Thus the element by itself is rank deficient, but this only manifests itself in problems for very thick plates and here only in certain cases. The two additional zero-energy modes are illustrated in Fig. IV-16. The first mode consists of $\theta_1 = \theta_2 = 0$ and an 'hourglass' pattern for w (see [38]). Modifying the one-point shear integration as indicated above removes the hourglass mode and leads to good results for very thick plates as evidenced by Figs. IV-9 and IV-10. The second mode consists of w = 0 and an in-plane twisting of the plate. In a mesh in which the rigid body modes are removed, this pattern cannot persist and thus causes no further rank deficiency.

7. Conclusions

We have presented an element for the bending of thin and moderately thick plates which involves minimal programming, is highly efficient and competitively accurate. Due to these attributes the element offers an attractive basis for nonlinear developments. Numerical sensitivity in applications involving extremely thin elements has been shown to be avoidable by employing a simple computational strategy. Very thick plates may be successfully analyzed by a slight modification to the element.

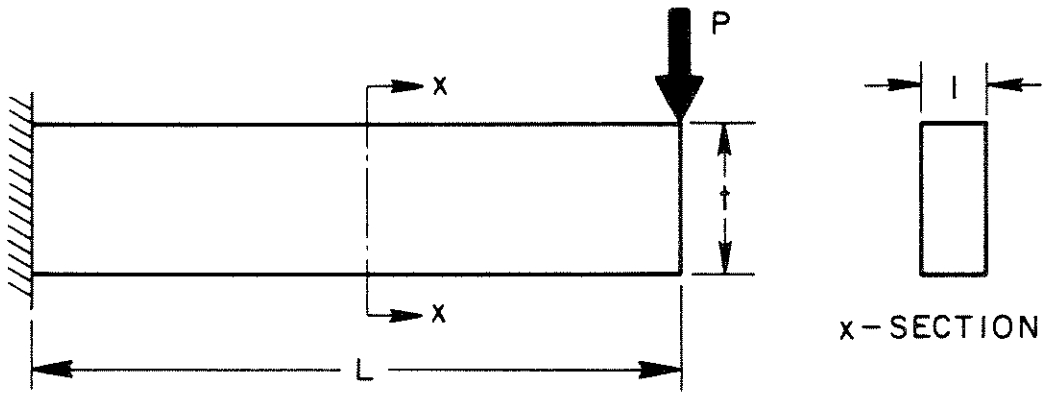

FIG. IV-1 CANTILEVER BEAM SUBJECTED TO END LOAD

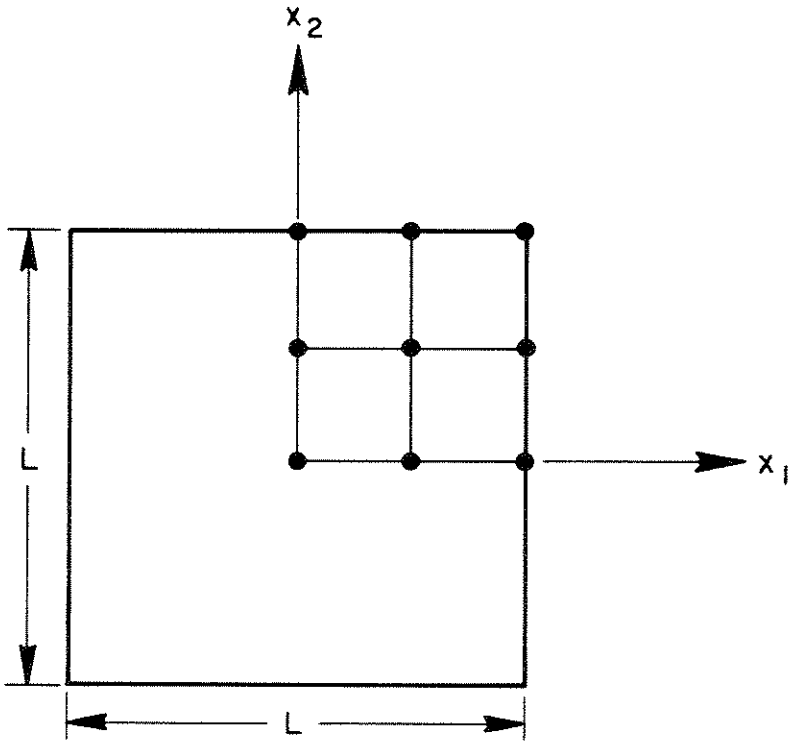

FIG. IV-2 SQUARE PLATE. DUE TO SYMMETRY ONLY ONE QUADRANT IS DISCRETIZED

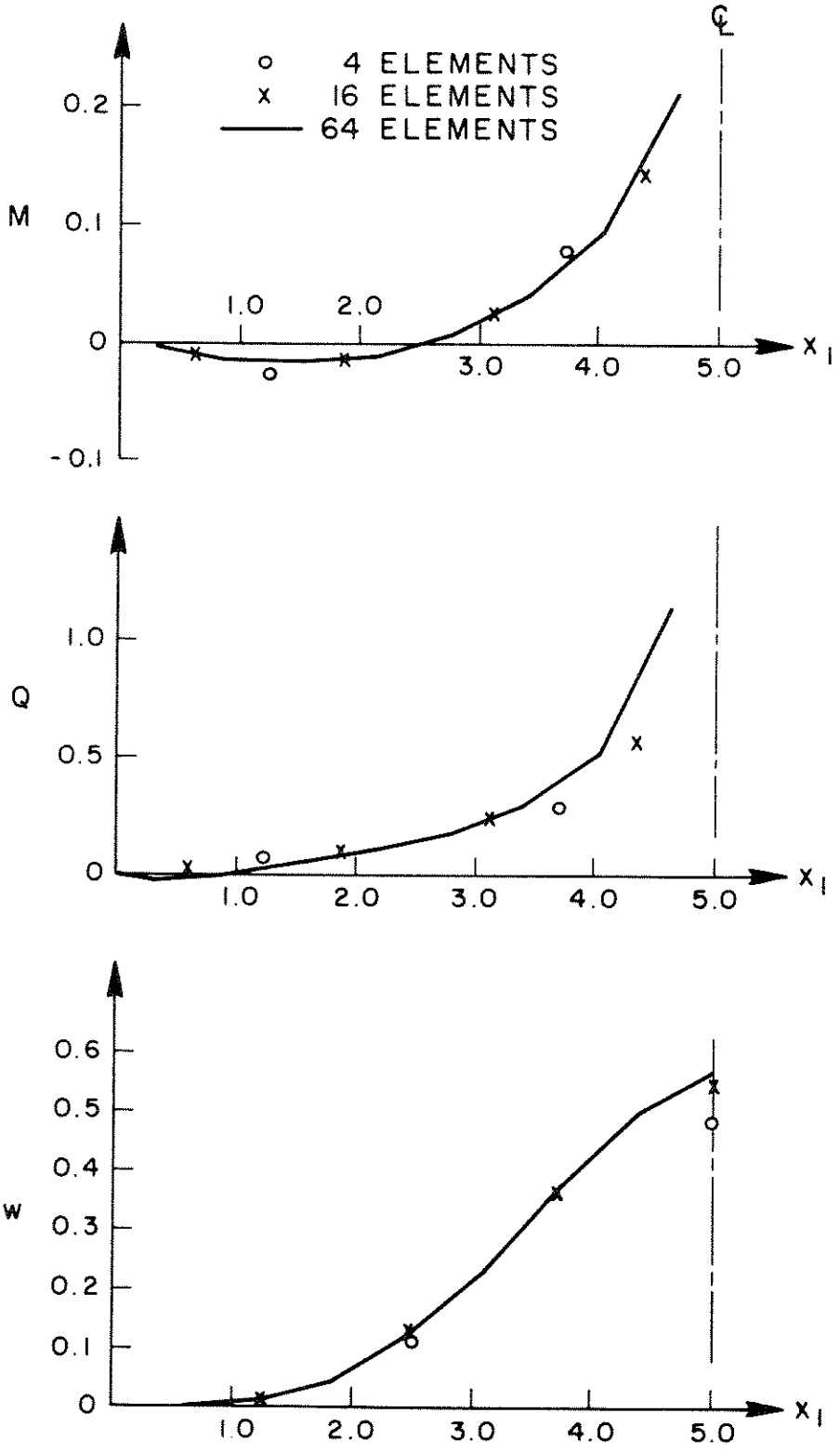

FIG. IV-3 MOMENT (M) SHEAR RESULTANT (Q) AND DISPLACEMENT (w) VERSUS EDGE COORDINATE (w_1) FOR A CLAMPED SQUARE PLATE SUBJECTED TO A

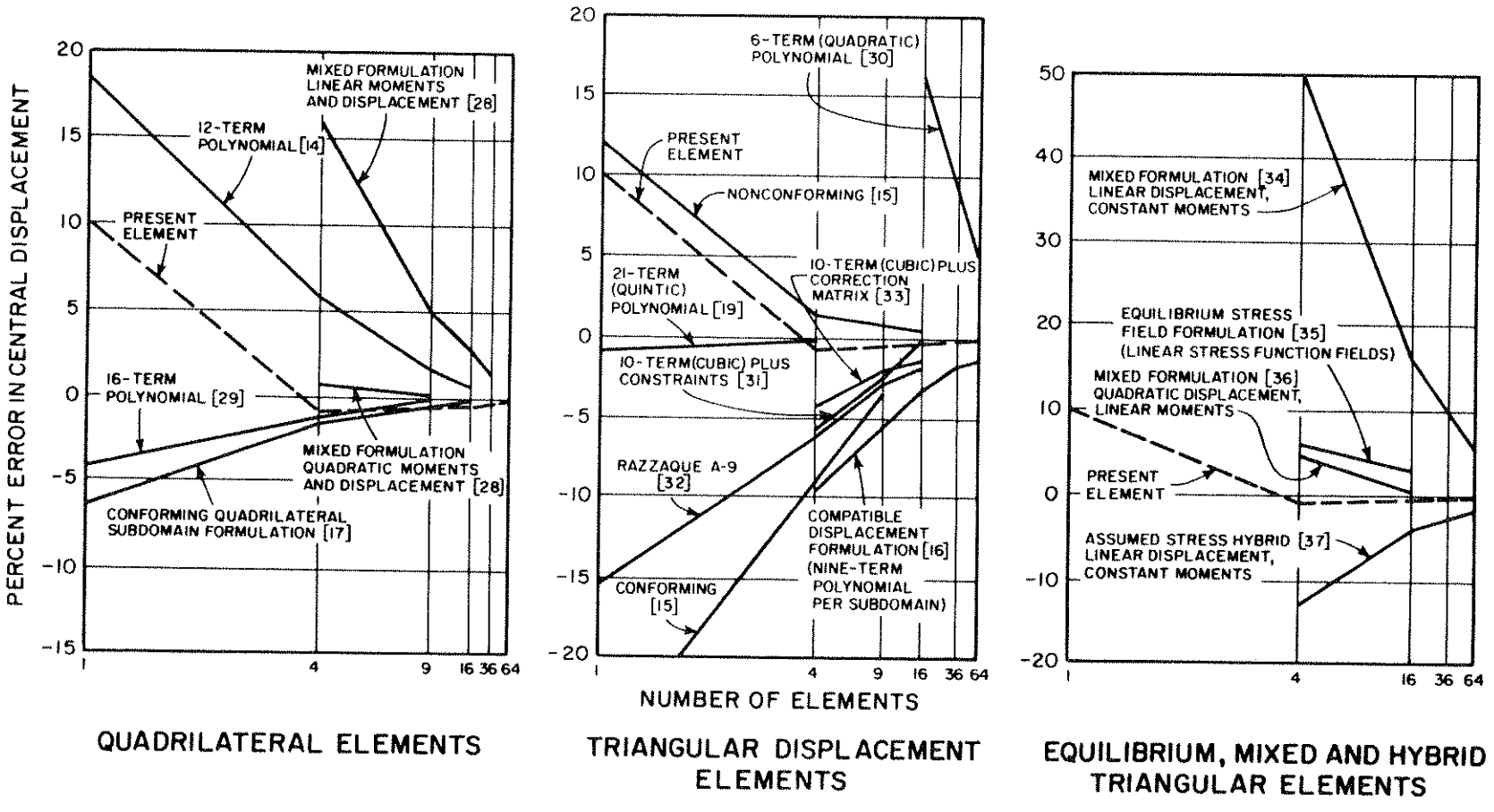

FIG. IV-4 SIMPLY SUPPORTED SQUARE PLATE SUBJECTED TO A CONCENTRATED LOAD. COMPARISION OF CENTER DISPLACEMENT FOR VARIOUS BENDING ELEMENTS

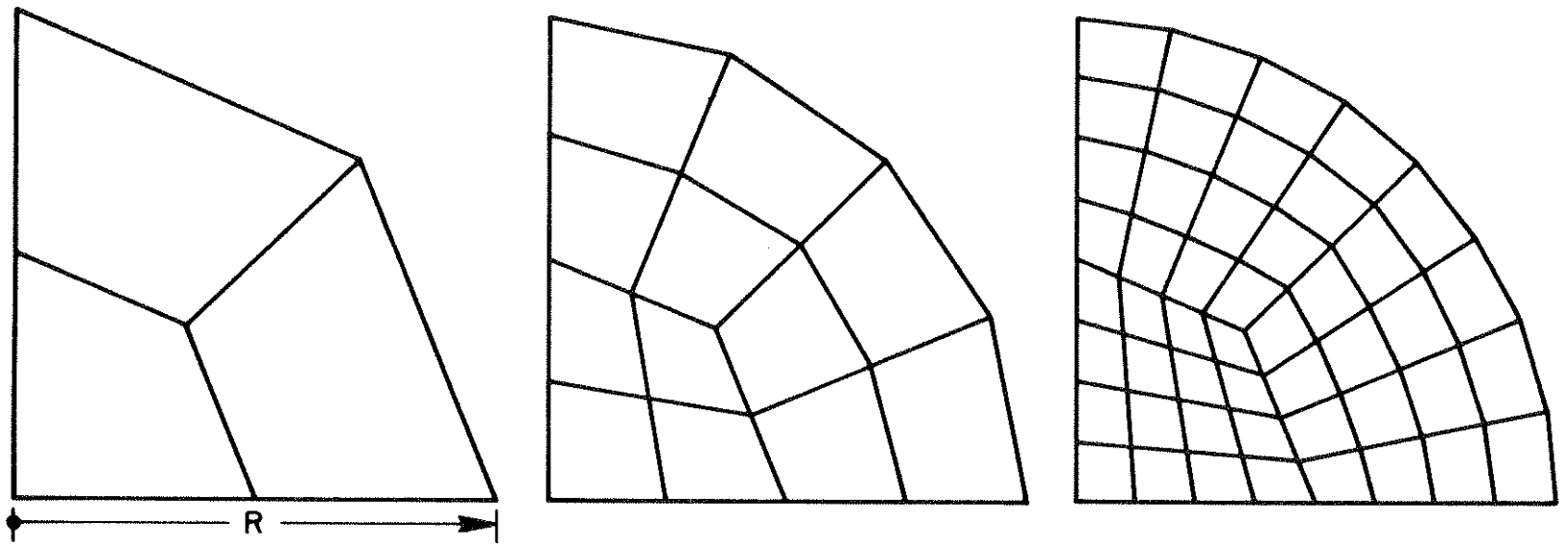

FIG. IV-5 FINITE ELEMENT MESHES FOR CLAMPED CIRCULAR PLATE. DUE DUE TO SYMMETRY ONE ONLY QUADRANT IS DISCRETIZED.

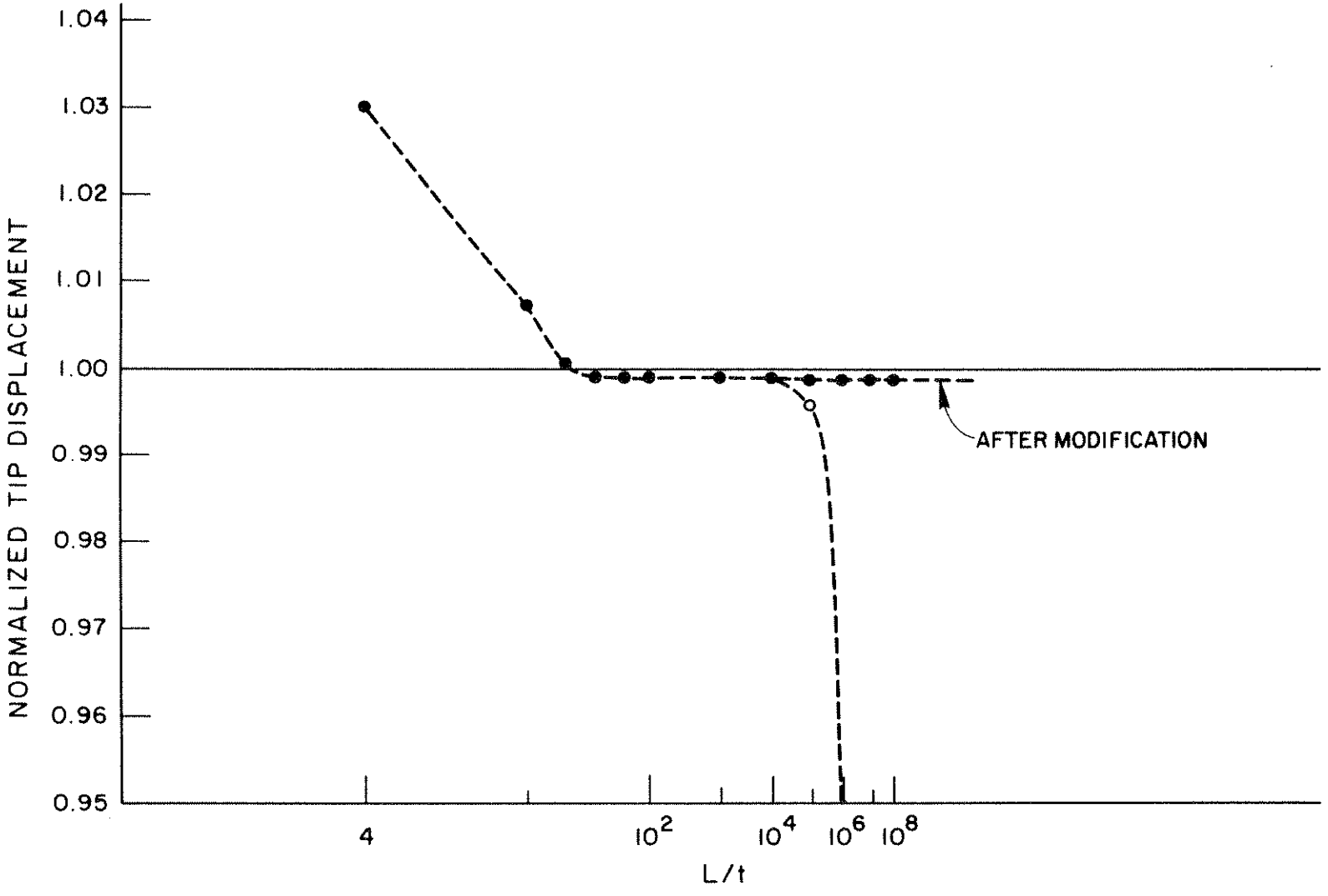

FIG. IV-6 16 ELEMENT CANTILEVER BEAM
SUBJECTED TO TIP LOAD.
NORMALIZED TIP DISPLACEMENT
VERSUS ASPECT RATIO

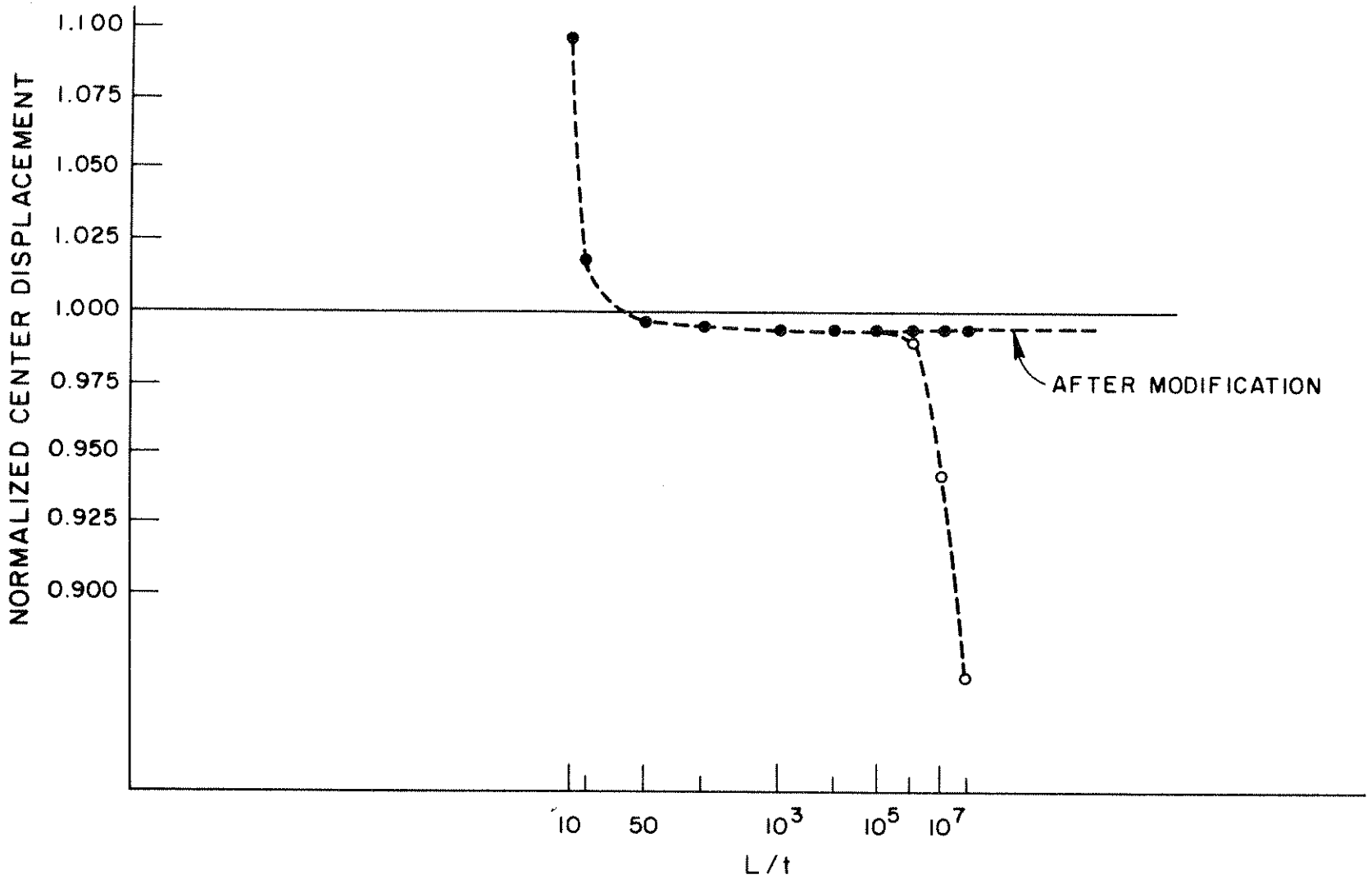

FIG. IV-7 16 ELEMENT MODEL OF SIMPLY SUPPORTED SQUARE PLATE SUBJECTED TO UNIFORM LOAD. NORMALIZED CENTER DISPLACEMENT VERSUS ASPECT RATIO

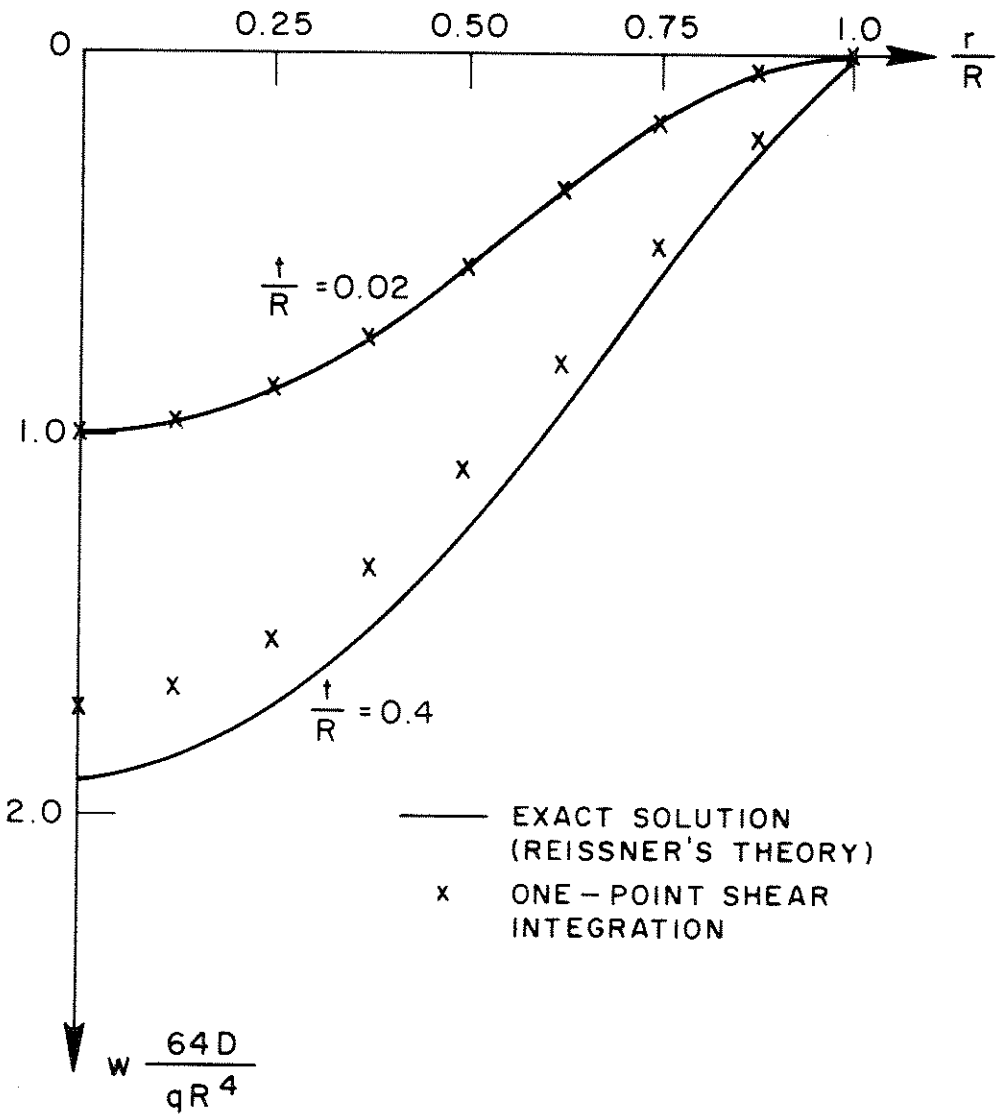

FIG. IV-8 CLAMPED CIRCULAR PLATE SUBJECTED TO UNIFORM LOAD (48 ELEMENT MODEL). COMPARISON OF UNDERINTEGRATED SHEAR ELEMENT WITH EXACT SOLUTION

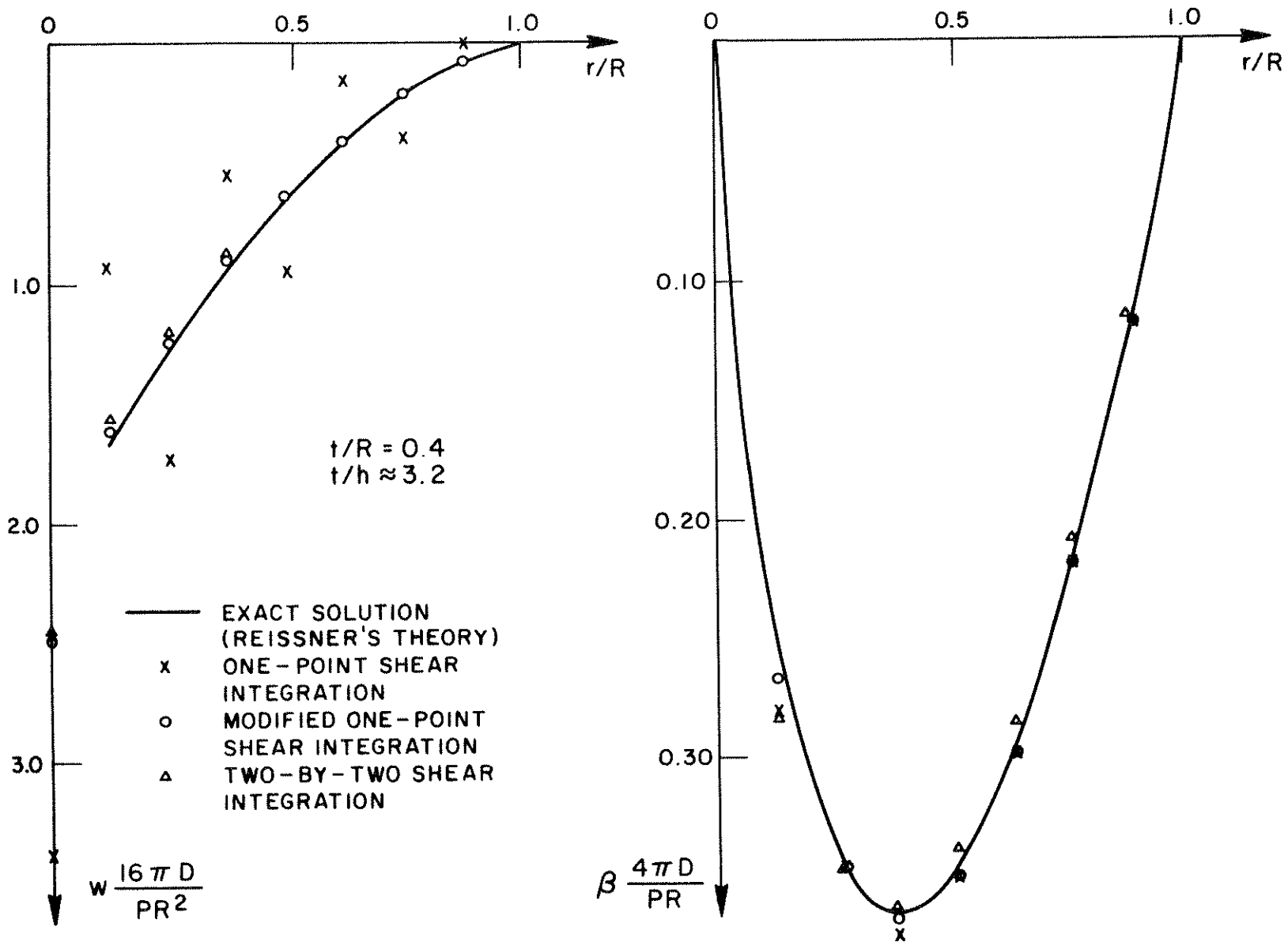

FIG. IV-9 CLAMPED CIRCULAR PLATE SUBJECTED TO CONCENTRATED LOAD (48 ELEMENT MODEL). COMPARISION OF UNDER-INTEGRATED SHEAR ELEMENTS WITH EXACT SOLUTION

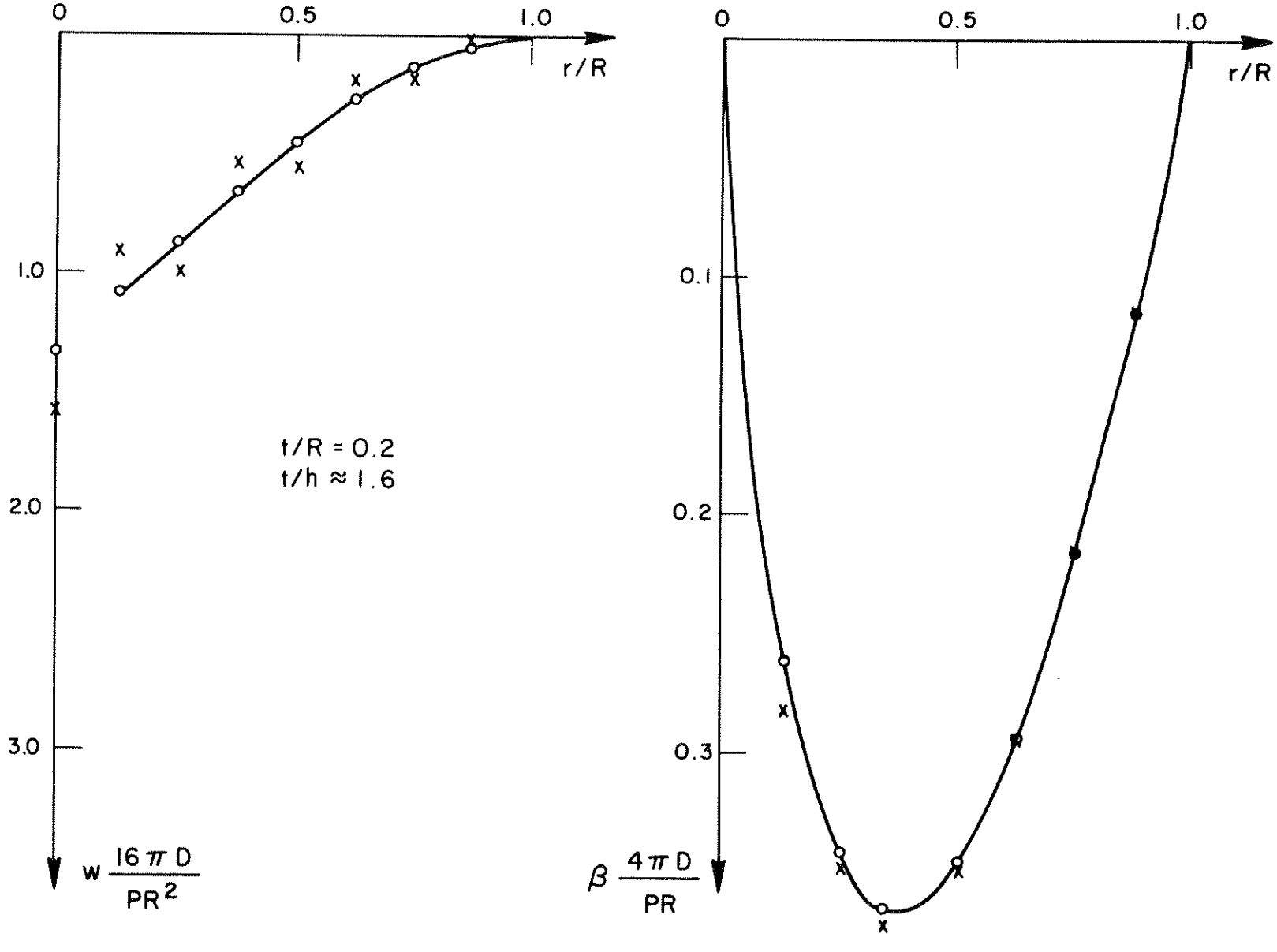

FIG. IV-10

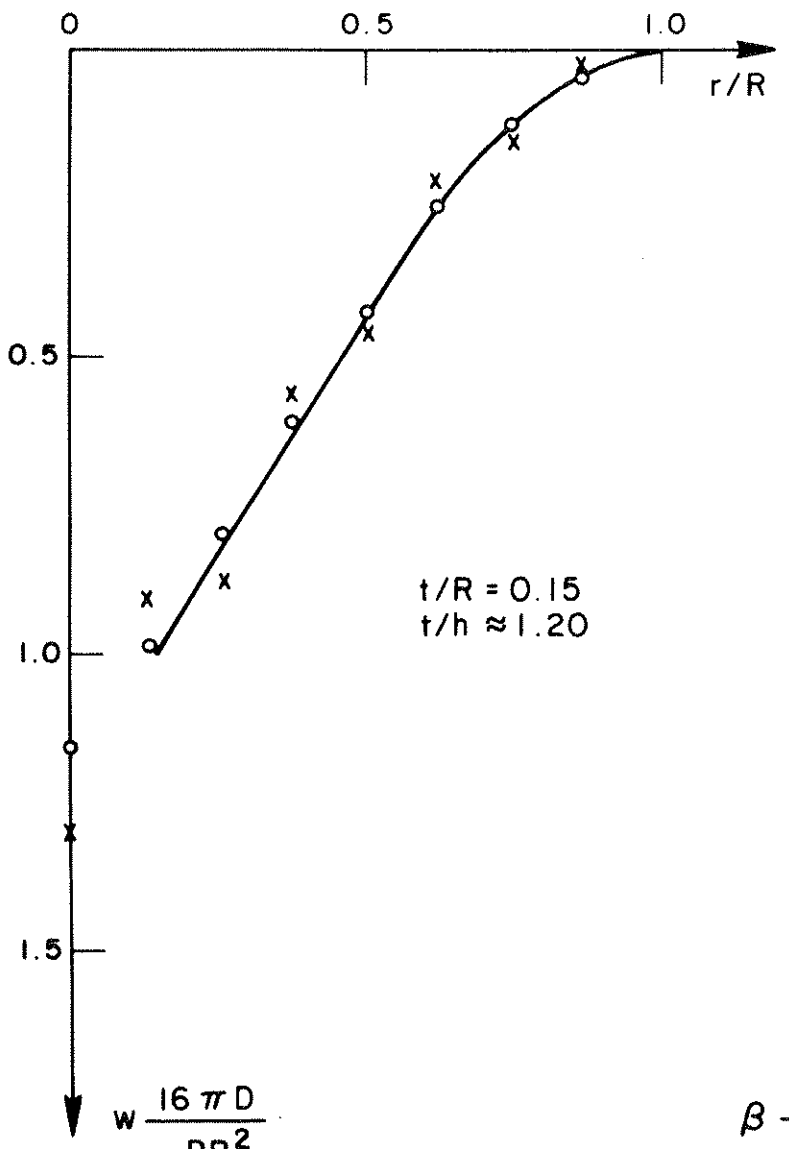
0
0.5
1.0
r/R
0.5
1.0
1.5
t/R = 0.15
t/h ≈ 1.20
w 16 π D / PR²

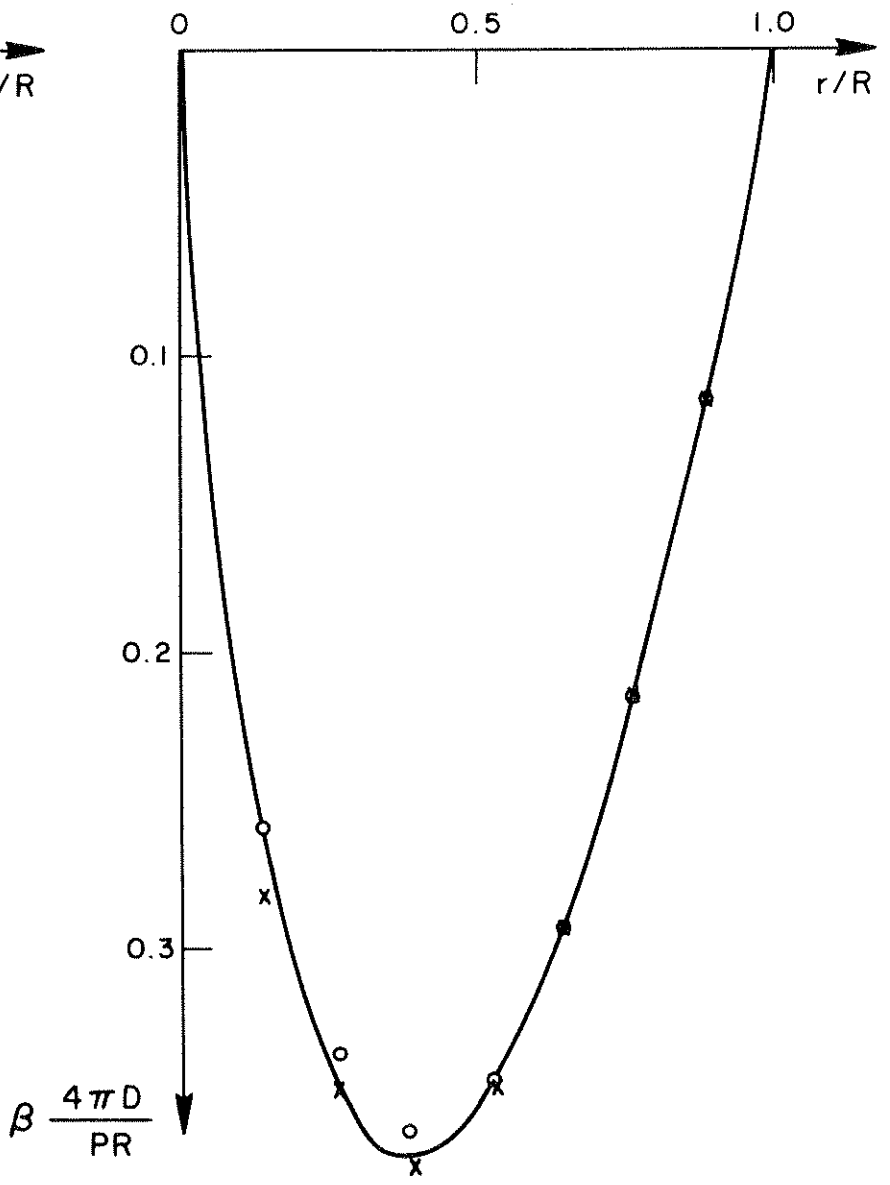
0
0.5
1.0
r/R
0.1
0.2
0.3
β 4 π D / PR

FIG. IV-11

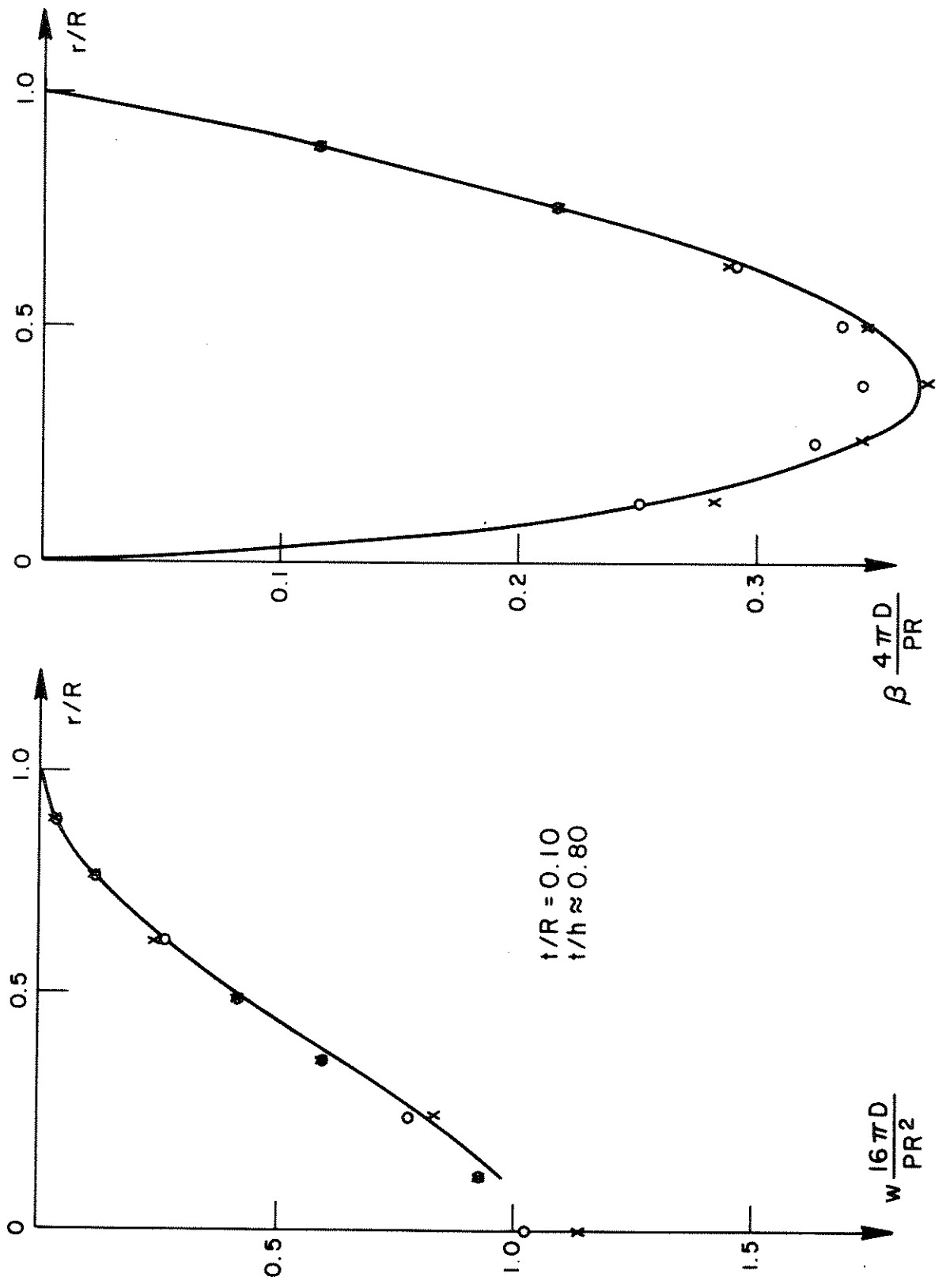
r/R
1.0
0.5
0
0.1
0.2
0.3
$\beta \frac{4\pi D}{PR}$
r/R
1.0
0.5
0
t/R = 0.10
t/h ≈ 0.80
0.5
1.0
1.5
$w \frac{16\pi D}{PR^2}$

FIG. IV-12

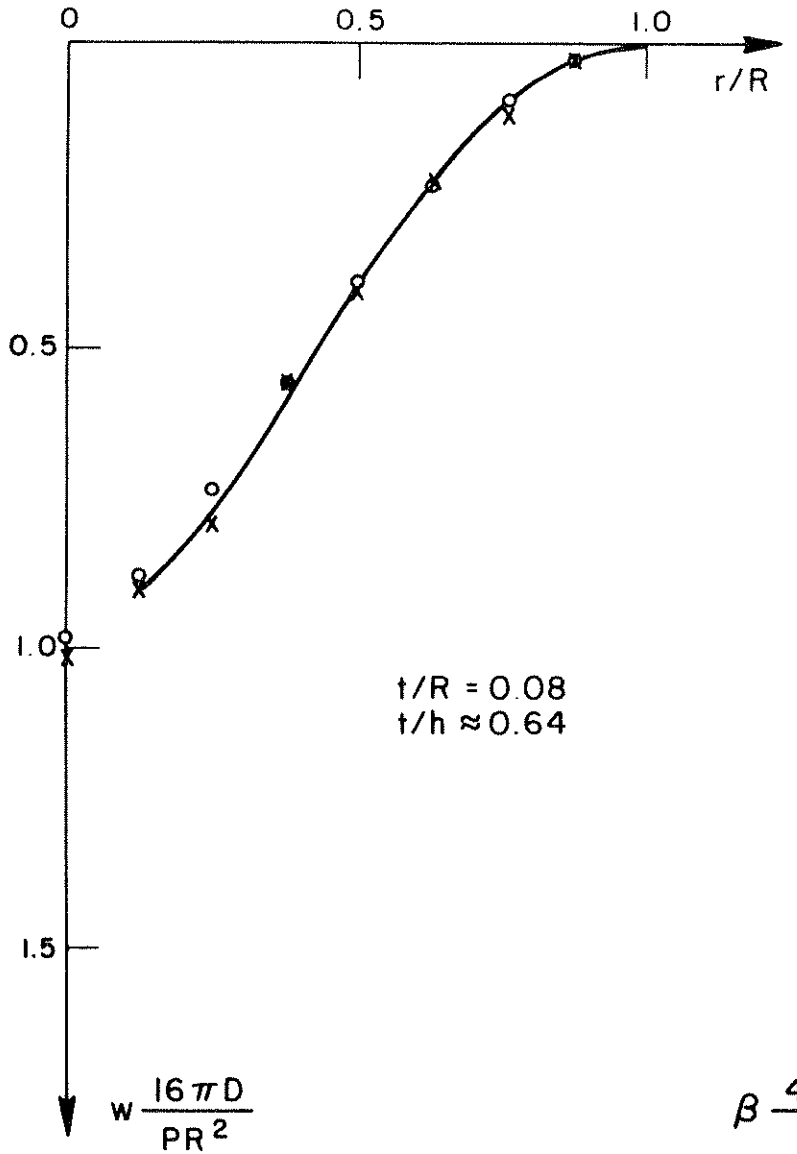
0
0.5
1.0
r/R
0.5
1.0
1.5
t/R = 0.08
t/h ≈ 0.64
w 16πD / PR²

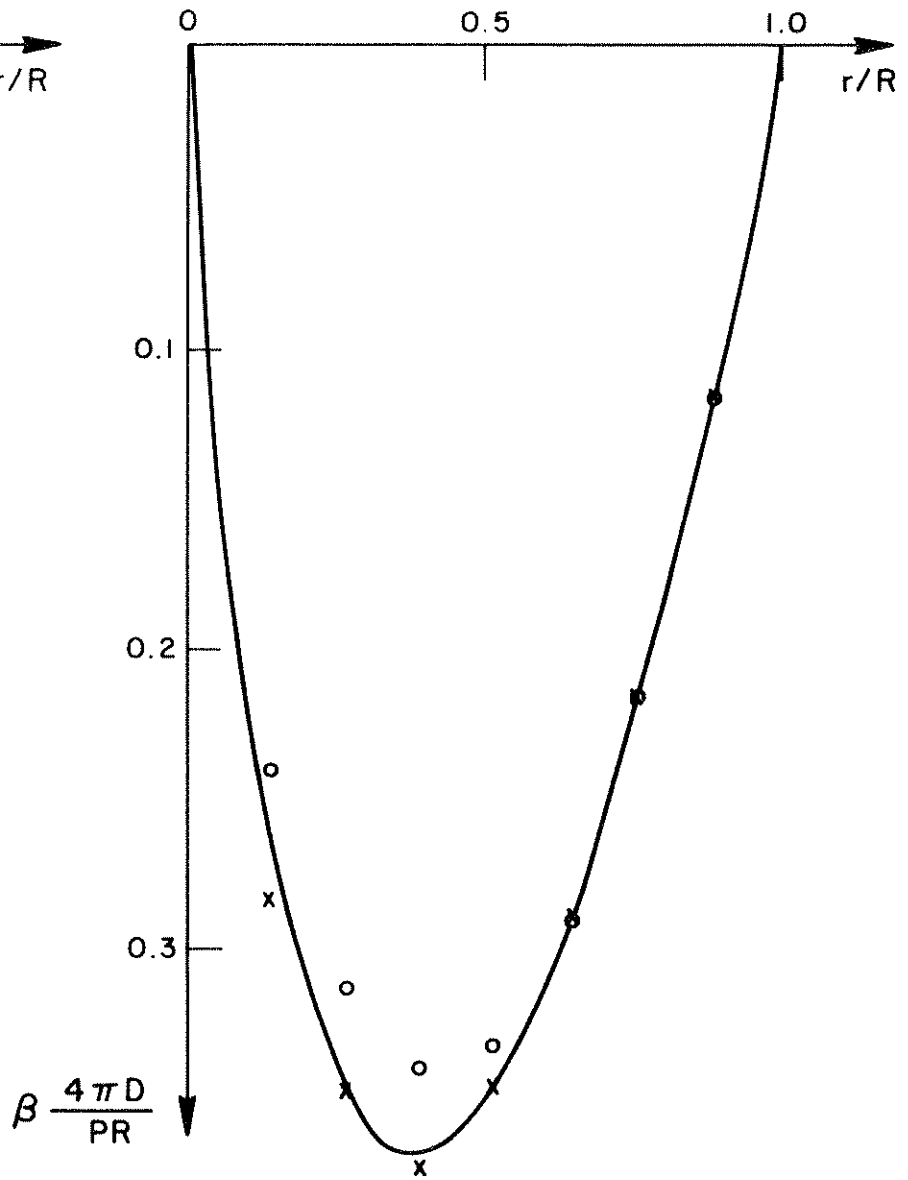
0
0.5
1.0
r/R
0.1
0.2
0.3
β 4πD / PR

FIG. IV-13

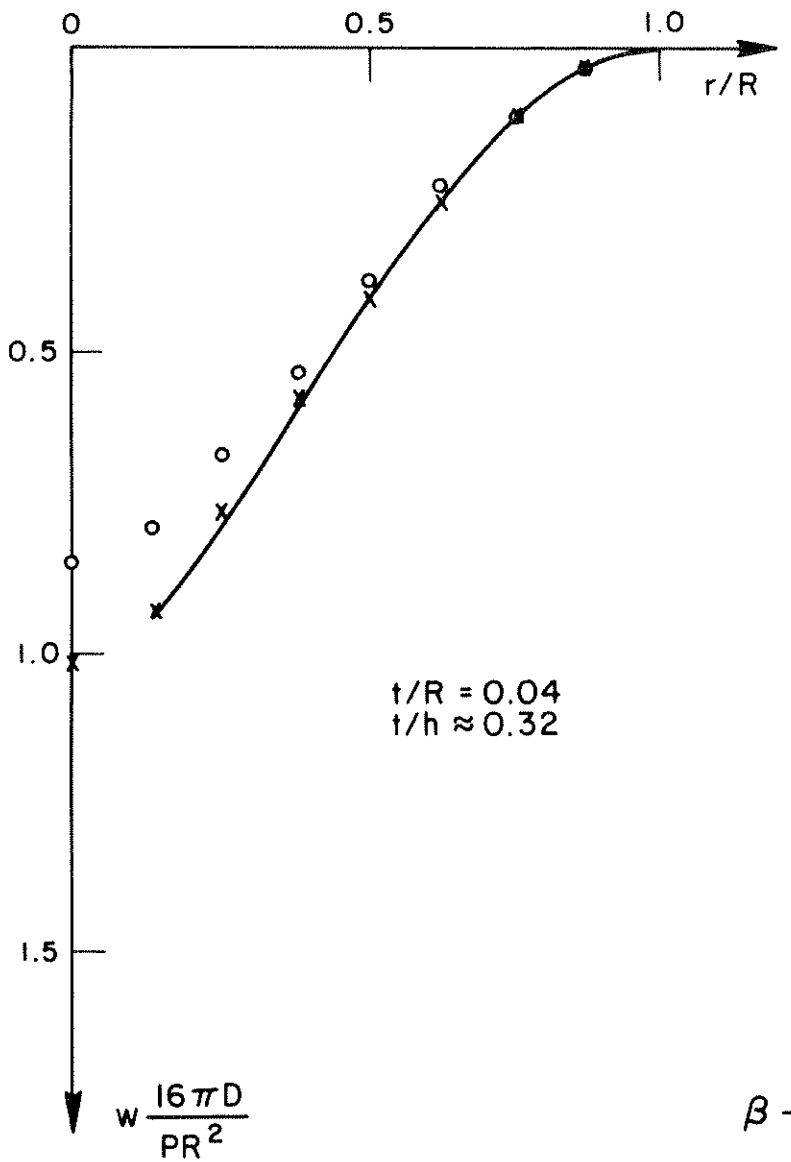
0
0.5
1.0
r/R
0.5
1.0
1.5
t/R = 0.04
t/h ≈ 0.32
$w\frac{16\pi D}{PR^2}$

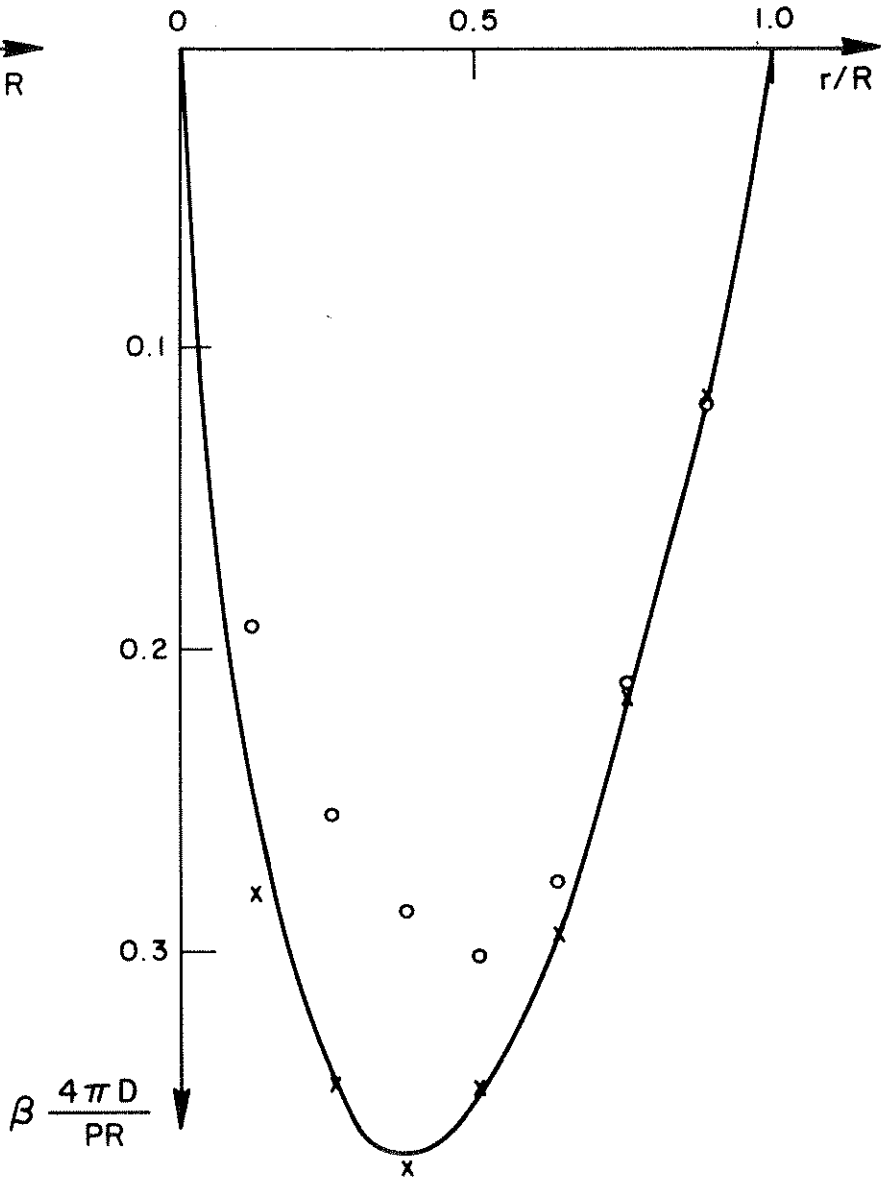
0
0.5
1.0
r/R
0.1
0.2
0.3
$\beta\frac{4\pi D}{PR}$

FIG. IV-14

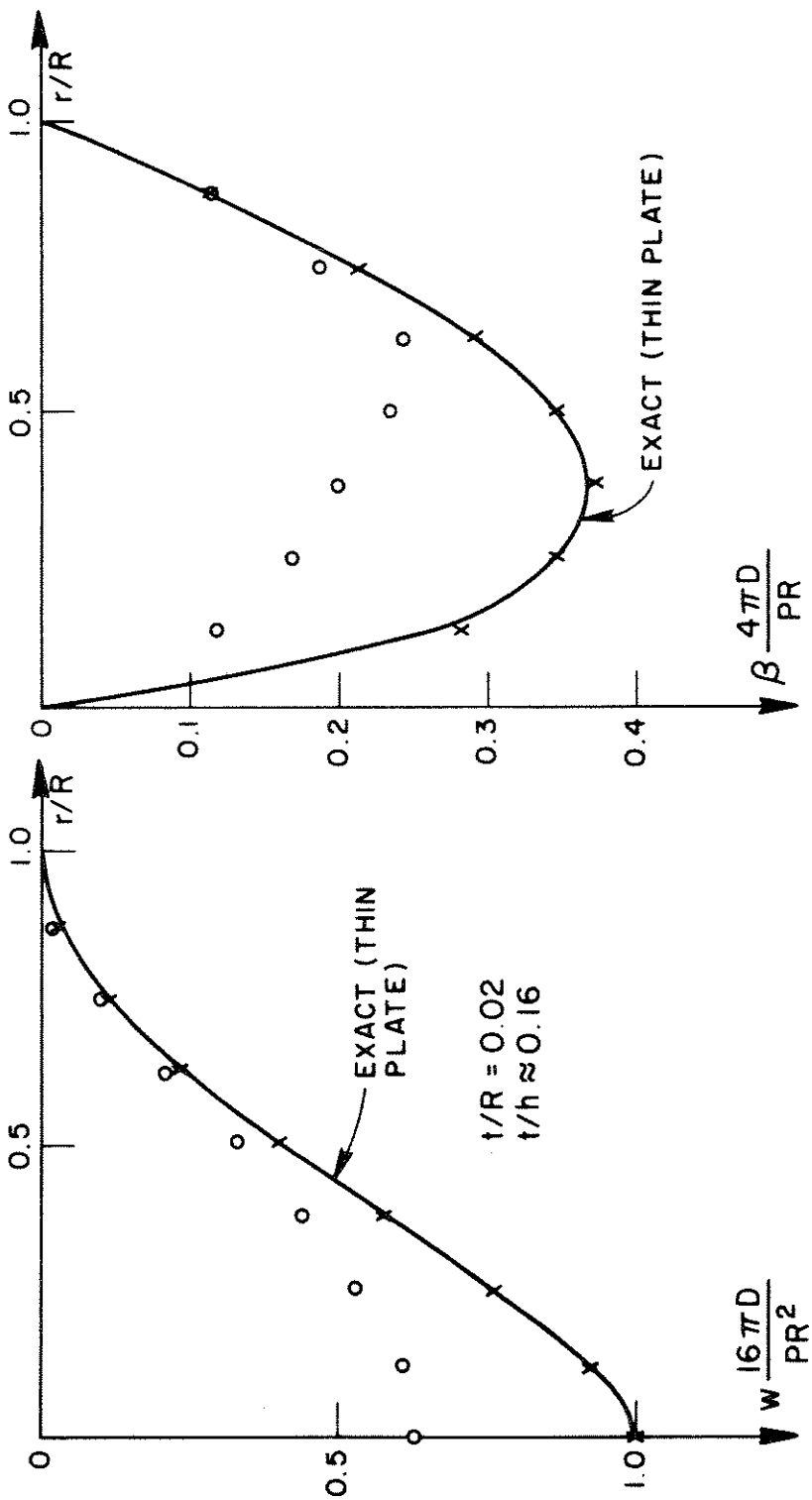
r/R
1.0
0.5
0
0.5
1.0
$w \frac{16\pi D}{PR^2}$
EXACT (THIN PLATE)
t/R = 0.02
t/h ≈ 0.16
r/R
1.0
0.5
0
0.1
0.2
0.3
0.4
$\beta \frac{4\pi D}{PR}$
EXACT (THIN PLATE)

FIG. IV-15

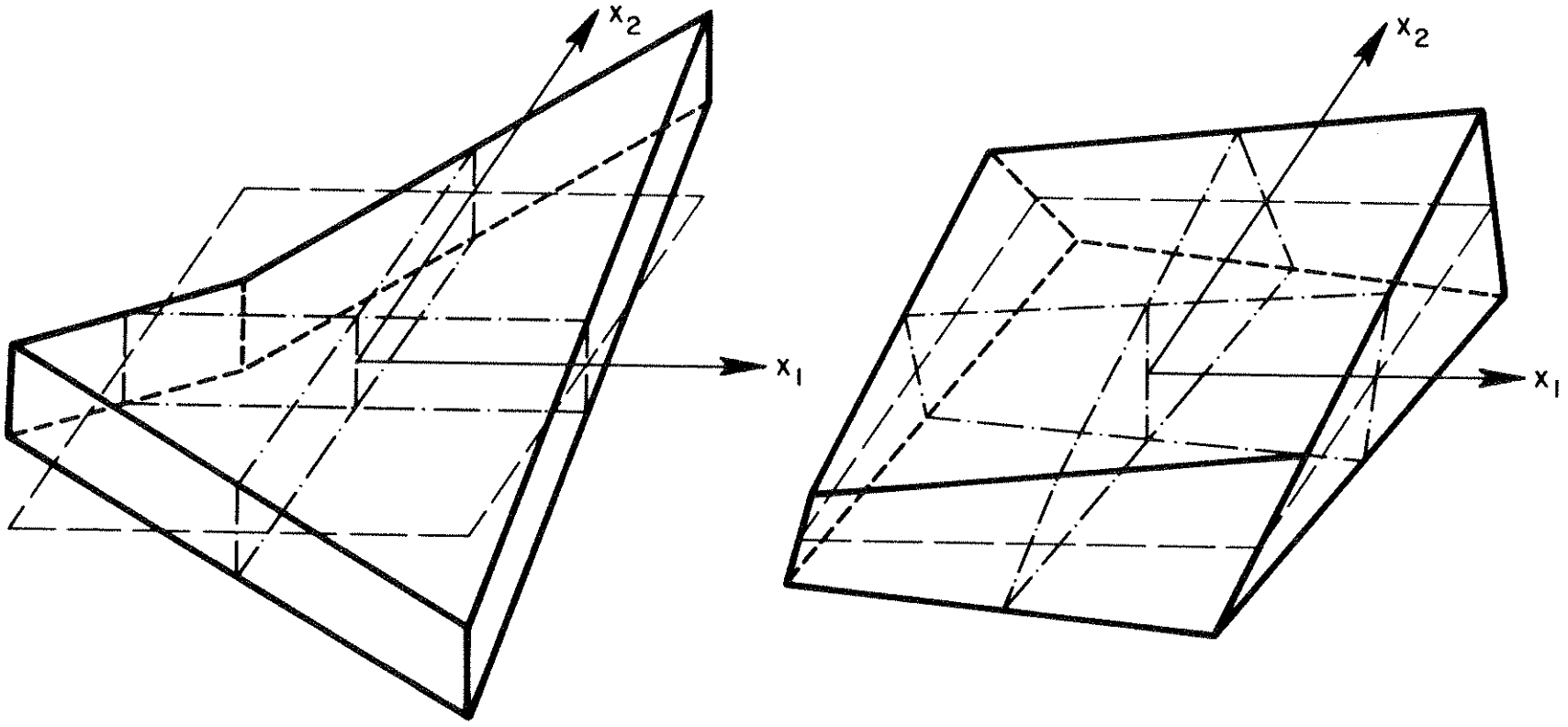

$w = x_1 x_2$

$\theta_1 = \theta_2 = 0$

MODE 1 HOURGLASS MODE

$w = 0$

$\theta_1 = -x_2$, $\theta_2 = x_1$

MODE 2 IN-PLANE TWIST MODE

FIG. IV-16 ZERO-ENERGY MODES OF UNDERINTEGRATED PLATE BENDING ELEMENT

References

1. T.J.R. Hughes, R.L. Taylor and J.L. Sackman, "Finite Element Formulation and Solution of Contact-Impact Problems in Continuum Mechanics." SESM Report No. 74-8, University of California, Berkeley (1974); copies can be obtained from National Technical Information Service, Springfield, Virginia, 22151, Accession No. PB-233 888/AS.

2. T.J.R. Hughes, R.L. Taylor and J.L. Sackman, "Finite Element Formulation and Solution of Contact-Impact Problems in Continuum Mechanics - II." SESM Report No. 75-3, University of California, Berkeley (1975).

3. T.J.R. Hughes, R.L. Taylor and J.L. Sackman, "Finite Element Formulation and Solution of Contact-Impact Problems in Continuum Mechanics - III." SESM Report No. 75-7, University of California, Berkeley (1975).

4. T.J.R. Hughes, R.L. Taylor, J.L. Sackman, A. Curnier and W. Kanoknukulchai, "Finite Element Formulation and Solution of a Class of Contact-Impact Problems in Continuum Mechanics." Transactions of the 3rd International Conference on Structural Mechanics in Reactor Technology, Paper J5/5, London (1975).

5. T.J.R. Hughes, R.L. Taylor, J.L. Sackman, A. Curnier and W. Kanoknukulchai, "A Finite Element Method for a Class of Contact-Impact Problems." Computational Methods in Applied Mechanics and Engineering (to appear).

6. J.D. Brooks and L.G. Rey, "Polystyrene-Urethane Composite Foam for Crash Padding Applications," Journal of Cellular Plastics, September/October, 232 (1973).

7. T.J.R. Hughes and H. Allik, "Finite Elements for Compressible and Incompressible Continua." Proc. Symp. Civil Eng., Vanderbilt University, Nashville, Tenn., 27-62 (1969).

8. T.J.R. Hughes, "Equivalence of Finite Elements for Nearly-Incompressible Elasticity" (to appear).

9. T.A. Shugar, "Transient Structural Response of the Linear Skull-Brain System," Proceedings of the Nineteenth Stapp Car Crash Conference, San Diego, California, November, 581-614 (1975).

10. O.C. Zienkiewicz, The Finite Element Method in Engineering Science, McGraw-Hill, New York (1971).

11. R.H. Gallagher, Finite Element Analysis Fundamentals, Prentice-Hall, Englewood Cliffs, New Jersey (1975).

12. R.D. Cook, Concepts and Applications of Finite Element Analysis, John Wiley and Sons, New York (1974).

13. B.M. Irons and K.J. Draper, "Inadequacy of Nodal Connections in a Stiffness Solution for Plate Bending," AIAA J, 3, 961 (1965).

14. R.J. Melosh, "Basis for Derivation of Matrices for the Direct Stiffness Method," AIAA J, 1, 1631-1637 (1963).

15. G.P. Bazely, Y.K. Cheung, B.M. Irons and O.C. Zienkiewicz, "Triangular Elements in Plate Bending--Conforming and Non-Conforming Solutions," Proceedings of the (First) Conference on Matrix Methods in Structural Mechanics, Wright-Patterson Air Force Base, Ohio, 547-576 (1965).

16. R.W. Clough and J.L. Tocher, "Finite Element Stiffness Matrices for Analysis of Plate Bending," Proceedings of the (First) Conference on Matrix Methods in Structural Mechanics, Wright-Patterson Air Force Base, Ohio, 515-545 (1965).

17. B. Fraeijs de Veubeke, "A Conforming Finite Element for Plate Bending," International Journal of Solids and Structures, 4, 95-108 (1968).

18. K. Bell, "A Refined Triangular Plate Bending Finite Element," International Journal for Numerical Methods in Engineering, 1, 101-122 (1969).

19. G.R. Cowper, E. Kosko, G. Lindberg and M. Olson, "Static and Dynamic Applications of a High Precision Triangular Plate Bending Element," AIAA J, 7, 1957-1965 (1969).

20. G. Butlin and R. Ford, "A Compatible Triangular Plate Bending Finite Element," International Journal of Solids and Structures, 6, 323-332 (1970).

21. T.H.H. Pian, "Element Stiffness Matrices for Boundary Compatibility and for Prescribed Boundary Stresses," Proceedings of the (First) Conference on Matrix Methods in Structural Mechanics, Wright-Patterson Air Force Base, Ohio, 457-478 (1965).

22. G. Wempner, J.T. Oden and D. Kross, "Finite Element Analysis of Thin Shells," Proceedings of the American Society of Civil Engineers, Journal of the Engineering Mechanics Division, 94, 1273-1294 (1968).

23. J.A. Stricklin, W.E. Haisler, P.R. Tisdale and R. Gunderson, "A Rapidly Converging Triangular Plate Bending Element," AIAA J, 7, 180-181 (1969).

24. I. Fried, "Shear in C^0 and C^1 Plate Bending Elements," International Journal of Solids and Structures, 9, 449-460 (1973).

25. I. Fried, "Residual Energy Balancing Technique in the Generation of Plate Bending Finite Elements," Computers and Structures, 771-778 (1974).

26. I. Fried and S.K. Yang, "Triangular, Nine-Degree-of-Freedom, C^0 Plate Bending Element of Quadratic Accuracy," Quarterly of Applied Mathematics, 31, 303-312 (1973).

27. O.C. Zienkiewicz, R.L. Taylor and J.M. Too, "Reduced Integration Technique in General Analysis of Plates and Shells," International Journal for Numerical Methods in Engineering, 3, 575-586 (1971).

28. J. Bron and G. Dhatt, "Mixed Quadrilateral Elements for Bending," AIAA J., 10, 1359-1361 (1972).

29. F.K. Bogner, R.L. Fox, and L.A. Schmit, "The Generation of Inter-element, Compatible Stiffness and Mass Matrices by the Use of Interpolation Formulas," Proc. (First) Conf. on Matrix Methods in Structural Mechanics, AFFDL TR 66-80, November (1965).

30. L.S.D. Morley, "The Constant-Moment Plate Bending Element," J. Strain Analysis, 6, 20-24 (1971).

31. J.W. Harvey and S. Kelsey, "Triangular Plate Bending Elements with Enforced Compatibility," AIAA J., 9, 1023-1026 (1971).

32. A.Q. Razzaque, "Program for Triangular Elements with Derivative Smoothing." International Journal Num. Meth. Eng., 6, 333-344 (1973).

33. F. Kikuchi and Y. Ando, "Some Finite Element Solutions for Plate Bending Problems by Simplified Hybrid Displacement Method," Nuc. Eng. Design, 23, 155-178 (1972).

34. L.R. Herrmann, "Finite Element Bending Analysis of Plates," J. Eng. Mech. Div., 94, 13-25 (1968).

35. Z.M. Elias, "Duality in Finite Element Methods," J. Eng. Mech. Div., 94, 931-946 (1968).

36. W. Visser, "A Refined Mixed-Type Plate Bending Element," AIAA J., 7, 1801-1802 (1969).

37. R.D. Cook, "Some Elements for Analysis of Plate Bending," J. Eng. Mech. Div., 98, 1452-1470 (1972).

38. S.W. Key, "A Finite Element Procedure for the Large Deformation Dynamic Response of Axisymmetric Solids," Computer Methods in Applied Mechanics and Engineering, 4, 195-218 (1974).

Division of Structural Engineering
and Structural Mechanics
Department of Civil Engineering

Report No. 76-4

FINITE ELEMENT MODELS FOR LARGE DISPLACEMENT CONTACT-IMPACT ANALYSIS

by

Thomas J.R. Hughes
Robert L. Taylor
Jerome L. Sackman
Worsak Kanoknukulchai

This report was prepared under
subcontract number

N68305-75-C-004

sponsored by

Civil Engineering Laboratory
Naval Construction Battalion Center
Port Hueneme, California

as part of

NHSTA Interagency Agreement Number

DOT-HS-5-01235

Funded by National Highway Traffic
Safety Administration
Department of Transportation

and

Funding Document Number

ONR 76-WR-60083

Funded by Office of Naval Research
Arlington, Virginia

July 1976